

Charged particles interaction in both a finite volume and a uniform magnetic field: II. Topological and analytic properties of a magnetic system

Peng Guo*  and Vladimir Gasparian

Department of Physics and Engineering, California State University, Bakersfield,
CA 93311, United States of America

E-mail: pguo@csub.edu

Received 14 February 2022, revised 24 April 2022

Accepted for publication 19 May 2022

Published 6 June 2022



CrossMark

Abstract

In present work, we extend Lüscher formula-like formalism to few-body system in a uniform magnetic field with Dirichlet boundary conditions. As a signature of non-trivial topological systems, the energy spectrum of topological edge states show up in the gap between allowed energy bands.

Keywords: lattice QCD, uniform magnetic field, Luscher formula

(Some figures may appear in colour only in the online journal)

1. Introduction

Study of few-body hadron/nuclear particles interaction and properties of few-body resonances is one of important subjects in modern physics. Hadron/nuclear particles provide the only means of understanding quantum chromodynamics (QCD), the underlying theory of quark and gluon interactions. However, making prediction of hadron/nuclear particle interactions from first principles is not always straightforward, due to the fact that most of theoretical computations are performed in various traps, for instance, periodic cubic box in lattice quantum chromodynamics (LQCD). As the result of trapped systems, only discrete energy spectrum is observed instead of scattering amplitudes. Hence, extracting infinite volume scattering amplitudes from discrete energy spectrum in a trapped system have become an important subject in LQCD and nuclear physics communities, see e.g. references [1–41]. When the size of a trap is much larger than the range of interactions, the short-range particles dynamics and long-range correlation effect due to the trap can be factorized. The connection between trapped system and infinite volume system are found in a closed form,

*Author to whom any correspondence should be addressed.

$$\det [\cot \delta(E) - \mathcal{M}(E)] = 0, \quad (1)$$

where $\delta(E)$ refers to the diagonal matrix of infinite volume scattering phase shifts, and the matrix function $\mathcal{M}(E)$ is associated to the geometry and dynamics of trap itself. The formula that has the form of equation (1) is known as Lüscher formula [1] in LQCD and Busch–Englert–Rzażewski–Wilchens formula [32] in a harmonic oscillator trap in nuclear physics community.

In preceding work [29], a Lüscher formula-like formalism was presented for a finite volume two-particle system in a uniform magnetic field. There are number of good reasons why study of a magnetic system in a finite volume might be interesting and desirable. In a broader content, external magnetic field plays important roles in cosmology, neutron star physics and heavy-ion phenomenology, see references [42, 43]. In QCD, magnetic field also produce number of interesting phenomena, such as, chiral magnetic effect [44–46] and magnetic catalysis which helps spontaneous breaking of non-abelian chiral symmetry [47, 48]. In addition, Landau level structure may turn charged ρ meson massless and QCD vacuum into a QCD superconductor [49]. Few-hadron systems in a uniform magnetic field can be studied by using background-field methods in lattice QCD [50–53]. The background-field method has already been applied to the computation of hadron magnetic polarizability in LQCD with the pion mass around 500 MeV [54, 55]. The magnetic polarizability of hadrons in LQCD are extracted by the mass shifts of particles measured both in the absence and presence of magnetic field. With heavy pion mass, the hadron resonances, such as ρ and $\Delta(1232)$, become stable particles. Masses of ρ and $\Delta(1232)$ are below $\pi\pi$ and πN thresholds respectively, hence decay of resonances can be safely neglected in LQCD computation. With lighter pion mass approaching physical pion mass around 140 MeV, these resonant hadron particles can no longer be treated as point-like particles, the few-body dynamics and hadron–hadron interactions may start playing significant roles. In addition to magnetic polarizability of hadron particles calculation in LQCD, the QCD phase structure in the presence of magnetic field, Landau level, topological Berry phase and related phenomena also have been active subjects of lattice QCD studies in recent years [56–61].

In LQCD simulation, periodic boundary condition has been a popular choice, which has the advantage of preserving discrete translational symmetry. In addition to periodic boundary condition, other boundary conditions have also been explored and used in LQCD for various purposes and applications, for example, using Dirichlet boundary condition (hard wall boundary condition) in recent LQCD studies of chiral symmetry restoration in [62] and magnetic/electric polarizability of hadrons in [54, 63–65]. In particular, Dirichlet boundary condition shows some advantages over periodic boundary in the LQCD study of magnetic and electric polarizability of hadron particles. For instance, Dirichlet boundary condition allows the implementation of nonquantized and small values of the uniform magnetic and electric field on lattice, see detailed discussion in references [54, 63–65].

In current work, Lüscher formula-like quantization conditions of two hadrons magnetic system with Dirichlet conditions are derived and presented. We will show that for a short-range interaction, the ultimate quantization condition with various boundary conditions, such as periodic and Dirichlet boundary conditions, can all be formulated in a similar form of equation (1). The boundary condition and finite volume effects are described by generalized magnetic zeta function. Such formalism may potentially be useful for the study of magnetic polarizability of hadron resonances when the few-body effect must be considered and the resonance can no longer be treated as a point-like particle, where Dirichlet boundary condition may be more preferable.

We also remark that although the LQCD computation with various boundary conditions has been our primary concerns in present work, it is worth mentioning that in the study of magnetic properties of quark–gluon and hadron matters and its response to external magnetic field, the effective QCD-like models, such as the Polyakov loops chiral linear-sigma model (PLSM) and Polyakov Nambu–Jona–Lasinio model (PNJL), also play the significant roles, see references [66–77]. To some extent, PLSM and PNJL are similar to LQCD but the size of a trap could be computationally better controlled.

The paper is organized as follows. The Lüscher formula-like quantization conditions with Dirichlet boundary conditions for two hadrons magnetic system are derived and presented in section 2. The discussions and summary are given in section 3.

2. Lüscher formula-like quantization conditions with Dirichlet boundary conditions

For a short-range interaction, the quantization conditions with various boundary conditions can all be presented in Lüscher formula-like form [1]. The details of derivation of Lüscher formula-like quantization conditions in a 2D plane with a periodic boundary condition can be found in appendix A, which applies to Dirichlet or other boundary conditions as well. Assuming S -wave dominance, the short-range interaction can be modeled by a contact interaction, the quantization condition is thus easily obtained,

$$\cot \delta_0(\varepsilon) = \mathcal{M}_B^{(2D)}(\mathbf{0}, \mathbf{0}; \varepsilon), \quad (2)$$

where the magnetic zeta function, $\mathcal{M}_B^{(2D)}$, describes the propagation of particles in a uniform magnetic field with proper boundary conditions. The S -wave phase shift, δ_0 , is associated with the short-range interaction between particles.

In follows, we first present the analytic solutions of 2D magnetic Green's functions with open, half open and hard wall boundary conditions in one direction and periodic in another in section 2.1. The associated magnetic zeta functions are given in section 2.2. The topological edge solutions exist in the 2D magnetic system with Dirichlet boundary condition, which may appear in the gap between bulk energy bands even with an impenetrable wall on the boundary. The spectrum of edge states vs bulk states is discussed in section 2.3.

2.1. Solutions of 2D magnetic Green's function with Dirichlet boundary conditions

Considering the propagation of two spinless hadron particles in a uniform magnetic field, the non-relativistic 2D magnetic Green's function with open, half open and hard wall boundary conditions in x -direction, but remaining the periodic boundary condition in y -direction, all have the form of

$$G_B^{(k_y \mathbf{e}_y, 2D)}(\boldsymbol{\rho}, \boldsymbol{\rho}'; \varepsilon) = \frac{1}{L} \sum_{p_y = \frac{2\pi n_y}{L} + k_y, n_y \in \mathbb{Z}} e^{ip_y(r_y - r'_y)} \times G_B^{(1D)}\left(r_x + \frac{p_y}{qB}, r'_x + \frac{p_y}{qB}; \varepsilon\right),$$

where

$$\boldsymbol{\rho} = r_x \mathbf{e}_x + r_y \mathbf{e}_y, \quad \boldsymbol{\rho}' = r'_x \mathbf{e}_x + r'_y \mathbf{e}_y$$

are relative coordinates defined in x – y plane. The wave vector k_y is related to center of mass (CM) momentum of two particles P_B by $k_y = \frac{P_{B,y}}{2}$. The 1D Green's function, $G_B^{(1D)}$, satisfies

differential equation

$$\left(\varepsilon + \frac{\partial_{r_x}^2}{2\mu} - \frac{(qB)^2}{2\mu} r_x^2\right) G_B^{(1D)}(r_x, r'_x; \varepsilon) = \delta(r_x - r'_x). \tag{4}$$

Before the boundary condition is implemented, equation (4) is parabolic cylinder equation type [78], the homogeneous parabolic cylinder equation has two independent solutions called parabolic cylinder functions [78]:

$$U\left(-\frac{\mu\varepsilon}{qB}, \pm\sqrt{2qB}r_x\right).$$

Therefore in general, the solution of $G_B^{(1D)}$ is given by

$$\begin{aligned} G_B^{(1D)}(r_x, r'_x; \varepsilon) &= \left[aU\left(-\frac{\mu\varepsilon}{qB}, \sqrt{2qB}r_{x<}\right) + bU\left(-\frac{\mu\varepsilon}{qB}, -\sqrt{2qB}r_{x<}\right) \right] \\ &\quad \times \left[cU\left(-\frac{\mu\varepsilon}{qB}, \sqrt{2qB}r_{x>}\right) + dU\left(-\frac{\mu\varepsilon}{qB}, -\sqrt{2qB}r_{x>}\right) \right], \end{aligned} \tag{5}$$

where $r_{x<}$ and $r_{x>}$ refer to the lesser and greater of (r_x, r'_x) respectively. All coefficients (a, b, c, d) are determined by boundary conditions and discontinuity relation

$$\partial_{r_x} G_B^{(1D)}(r_x, r'_x; \varepsilon) \Big|_{r_x=r'_x-0}^{r_x=r'_x+0} = 2\mu. \tag{6}$$

2.1.1. Open boundary in x-direction. With open boundary condition in x -direction, using properties of parabolic cylinder functions,

$$U\left(-\frac{\mu\varepsilon}{qB}, z\right) \xrightarrow{z \rightarrow \infty} 0, \quad U\left(-\frac{\mu\varepsilon}{qB}, -z\right) \xrightarrow{z \rightarrow \infty} \infty, \tag{7}$$

the coefficients $a = 0$ and $d = 0$. Also using equation (6) and relation

$$\mathcal{W}\left\{U\left(-\frac{\mu\varepsilon}{qB}, z\right), U\left(-\frac{\mu\varepsilon}{qB}, -z\right)\right\} = \frac{\sqrt{2\pi}}{\Gamma\left(\frac{1}{2} - \frac{\mu\varepsilon}{qB}\right)}, \tag{8}$$

where $\mathcal{W}(f, g) = fg' - gf'$ stands for the Wronskian of two functions, so we obtain

$$\begin{aligned} G_B^{(\text{Open}, 1D)}(r_x, r'_x; \varepsilon) &= -2\mu \frac{\Gamma\left(\frac{1}{2} - \frac{\mu\varepsilon}{qB}\right)}{\sqrt{2qB}\sqrt{2\pi}} \\ &\quad \times U\left(-\frac{\mu\varepsilon}{qB}, -\sqrt{2qB}r_{x<}\right) U\left(-\frac{\mu\varepsilon}{qB}, \sqrt{2qB}r_{x>}\right). \end{aligned} \tag{9}$$

Considering another representation of open boundary condition 2D magnetic Green's function,

$$G_B^{(\text{Open}, k_y \mathbf{e}_y, 2\text{D})}(\boldsymbol{\rho}, \boldsymbol{\rho}'; \varepsilon) = \sum_{n_y} e^{-ik_y n_y L} G_B^{(\infty, 2\text{D})}(\boldsymbol{\rho} + n_y L \mathbf{e}_y, \boldsymbol{\rho}'; \varepsilon), \quad (10)$$

we can also conclude that in addition to equation (A13), another representation of $G_B^{(\infty, 2\text{D})}$ is given by

$$\begin{aligned} G_B^{(\infty, 2\text{D})}(\boldsymbol{\rho}, \boldsymbol{\rho}'; \varepsilon) &= -2\mu \frac{\Gamma\left(\frac{1}{2} - \frac{\mu\varepsilon}{qB}\right)}{\sqrt{2qB}\sqrt{2\pi}} \int_{-\infty}^{\infty} \frac{dp_y}{2\pi} e^{ip_y(r_y - r'_y)} \\ &\times U\left(-\frac{\mu\varepsilon}{qB}, -\sqrt{2qB}\left(r_{x<} + \frac{p_y}{qB}\right)\right) \\ &\times U\left(-\frac{\mu\varepsilon}{qB}, \sqrt{2qB}\left(r_{x>} + \frac{p_y}{qB}\right)\right). \end{aligned} \quad (11)$$

Similar result and some interesting discussion of quasi-classical approximation of $G_B^{(\infty, 2\text{D})}$ can be found in [79].

2.1.2. Half open boundary in x-direction. Next, let us consider only putting one hard wall on one side, e.g.

$$G_B^{(\text{Half}, k_y \mathbf{e}_y, 2\text{D})}(\boldsymbol{\rho}, \boldsymbol{\rho}'; \varepsilon)|_{r_{x>} \geq \frac{n_q L}{2} \mathbf{e}_x} = 0. \quad (12)$$

Using equation (7) again, we can eliminating $U\left(-\frac{\mu\varepsilon}{qB}, \sqrt{2qB}r_{x<}\right)$ term in equation (5). The rest of coefficients can be determined by implementing boundary condition and using equation (8) again, we thus find

$$\begin{aligned} G_B^{(\text{Half}, 1\text{D})}(r_x, r'_x; \varepsilon) &= -2\mu \frac{\Gamma\left(\frac{1}{2} - \frac{\mu\varepsilon}{qB}\right)}{\sqrt{2qB}\sqrt{2\pi}} \\ &\times U\left(-\frac{\mu\varepsilon}{qB}, -\sqrt{2qB}r_{x<}\right) \left[U\left(-\frac{\mu\varepsilon}{qB}, \sqrt{2qB}r_{x>}\right) \right. \\ &\left. - \frac{U\left(-\frac{\mu\varepsilon}{qB}, \sqrt{2qB}\frac{L_+}{2}\right)}{U\left(-\frac{\mu\varepsilon}{qB}, -\sqrt{2qB}\frac{L_+}{2}\right)} U\left(-\frac{\mu\varepsilon}{qB}, -\sqrt{2qB}r_{x>}\right) \right], \end{aligned} \quad (13)$$

where

$$\frac{L_+}{2} = \frac{n_q L}{2} + \frac{p_y}{qB}. \quad (14)$$

2.1.3. Hard wall boundary in x-direction. At last, let us consider putting hard walls on both sides, e.g.

$$G_B^{(\text{h.w.}, k_y \mathbf{e}_y, 2\text{D})}(\boldsymbol{\rho}, \boldsymbol{\rho}'; \varepsilon)|_{r_{x<} \leq -\frac{n_q L}{2} \mathbf{e}_x, r_{x>} \geq \frac{n_q L}{2} \mathbf{e}_x} = 0. \quad (15)$$

Again, implementing boundary condition and using equation (8), we find

$$\begin{aligned}
G_B^{(\text{h.w.,1D})}(r_x, r'_x; \varepsilon) &= \frac{2\mu \frac{\Gamma\left(\frac{1}{2} - \frac{\mu\varepsilon}{qB}\right)}{\sqrt{2qB}\sqrt{2\pi}}}{\frac{U\left(-\frac{\mu\varepsilon}{qB}, -\sqrt{2qB}\frac{L_+}{2}\right)}{U\left(-\frac{\mu\varepsilon}{qB}, \sqrt{2qB}\frac{L_+}{2}\right)} - \frac{U\left(-\frac{\mu\varepsilon}{qB}, \sqrt{2qB}\frac{L_-}{2}\right)}{U\left(-\frac{\mu\varepsilon}{qB}, -\sqrt{2qB}\frac{L_-}{2}\right)}} \\
&\times \left[U\left(-\frac{\mu\varepsilon}{qB}, -\sqrt{2qB}r_{x<}\right) \right. \\
&\quad \left. - \frac{U\left(-\frac{\mu\varepsilon}{qB}, \sqrt{2qB}\frac{L_-}{2}\right)}{U\left(-\frac{\mu\varepsilon}{qB}, -\sqrt{2qB}\frac{L_-}{2}\right)} U\left(-\frac{\mu\varepsilon}{qB}, \sqrt{2qB}r_{x<}\right) \right] \\
&\times \left[U\left(-\frac{\mu\varepsilon}{qB}, -\sqrt{2qB}r_{x>}\right) \right. \\
&\quad \left. - \frac{U\left(-\frac{\mu\varepsilon}{qB}, -\sqrt{2qB}\frac{L_+}{2}\right)}{U\left(-\frac{\mu\varepsilon}{qB}, \sqrt{2qB}\frac{L_+}{2}\right)} U\left(-\frac{\mu\varepsilon}{qB}, \sqrt{2qB}r_{x>}\right) \right], \tag{16}
\end{aligned}$$

where

$$\frac{L_-}{2} = \frac{n_q L}{2} - \frac{p_y}{qB}. \tag{17}$$

2.2. Solutions of 2D magnetic zeta functions with Dirichlet boundary conditions

It has been well-known in condensed matter physics that Bloch particles in a magnetic field exhibit the non-trivial topological properties, see reference [80] and also appendix B. For instance, the magnetic field forces a wavefunction of Bloch particles to develop vortices in crystal momentum space [81]. The phase of wavefunction of Bloch particles is not well-defined throughout entire magnetic Brillouin zone, which is associated to a non-trivial topology of a magnetic system. When crystal momentum of a Bloch particle is forced to circle around the vortices, non-zero vorticity is ultimately related to quantized Hall conductance [81, 82].

One of important consequences of a non-trivial topological system is the existence of gapless topological edge states that occur in the energy gap between the bulk bands [83–85]. The study of conventional edge or surface states in fact has a long history [86, 87], the boundary effect may cause the localization of state near the edge or surface of material. Though the energy spectrum of a system with a penetrable boundary may protrude into the gap between bulk bands, for topologically trivial systems, the eigen-energies of an impenetrable wall on boundary are only situated on the edge of bulk energy bands. This fact can be illustrated with a 2D non-magnetic system with different boundary conditions. In the absence of magnetic field, the 2D finite volume Green's function that satisfies periodic boundary conditions in both x and y directions is given by

$$G_0^{(L,\mathbf{k},2\text{D})}(\boldsymbol{\rho}; \varepsilon) = \frac{1}{L^2} \sum_{\mathbf{p} = \frac{2\pi\mathbf{n}}{L} + \mathbf{k}, \mathbf{n} \in \mathbb{Z}^2} \frac{e^{i\mathbf{p}\cdot\boldsymbol{\rho}}}{\varepsilon - \frac{\mathbf{p}^2}{2\mu}}, \tag{18}$$

compared with

$$G_0^{(\text{h.w.}, k_y \mathbf{e}_y, 2\text{D})}(\boldsymbol{\rho}, \boldsymbol{\rho}'; \varepsilon) = \frac{1}{L} \sum_{p_y = \frac{2\pi n_y}{L} + k_y, n_y \in \mathbb{Z}} e^{ip_y(r_y - r'_y)} \times 2\mu \frac{\sin \sqrt{2\mu\varepsilon - p_y^2} (r_{y>} - \frac{L}{2}) \sin \sqrt{2\mu\varepsilon - p_y^2} (r_{y<} + \frac{L}{2})}{\sqrt{2\mu\varepsilon - p_y^2} \sin \sqrt{2\mu\varepsilon - p_y^2} L}, \quad (19)$$

which satisfies hard wall boundary condition in x -direction but still remains periodic in y -direction,

$$G_0^{(\text{h.w.}, k_y \mathbf{e}_y, 2\text{D})}(\boldsymbol{\rho}, \boldsymbol{\rho}'; \varepsilon)|_{\boldsymbol{\rho}, \boldsymbol{\rho}' = \pm \frac{L}{2} \mathbf{e}_x} = 0. \quad (20)$$

Therefore, with a contact interaction,

$$V(\boldsymbol{\rho}) = V_0 \delta(\boldsymbol{\rho}),$$

and using equation (18) and identity

$$\frac{1}{L} \sum_{p_x = \frac{2\pi n_x}{L} + k_x, n_x \in \mathbb{Z}} \frac{1}{q^2 - p_x^2} = \frac{\cot \frac{q - k_x}{2} L + \cot \frac{q + k_x}{2} L}{4q}, \quad (21)$$

the bulk energy band solutions with periodic boundary condition along both directions are determined by

$$\frac{1}{V_0} = \frac{2\mu}{L} \sum_{p_y = \frac{2\pi n_y}{L} + k_y, n_y \in \mathbb{Z}} \frac{\cot \frac{\sqrt{2\mu\varepsilon - p_y^2} - k_x}{2} L + \cot \frac{\sqrt{2\mu\varepsilon - p_y^2} + k_x}{2} L}{4\sqrt{2\mu\varepsilon - p_y^2}}. \quad (22)$$

Using equation (19), the edge solutions with hard wall boundary condition along x -direction are determined by

$$\frac{1}{V_0} = \frac{2\mu}{L} \sum_{p_y = \frac{2\pi n_y}{L} + k_y, n_y \in \mathbb{Z}} \frac{\cot \frac{\sqrt{2\mu\varepsilon - p_y^2} - \frac{\pi}{L}}{2} L}{2\sqrt{2\mu\varepsilon - p_y^2}}. \quad (23)$$

We can see clearly that for a fixed k_y and V_0 , the edge solution is only part of bulk energy band solutions with special value of wave vector $k_x = \frac{\pi}{L}$, which indeed sit at the edge of bulk energy bands. On the contrary, even with impenetrable walls on the boundary, the topological edge states may appear in the gap between bulk energy bands.

For a magnetic two-hadron systems in general, the energy spectrum for various boundary conditions must be generated by using equation (A55). The topological edge states in gaps between allowed energy bands in fact can be illustrated by only considering a simple case with only a single scatter placed at origin ($n_q = 1$). Even so, it is sufficient to demonstrate the difference between edge state solutions and bulk state solutions.

The magnetic zeta function for various boundary condition can be defined similarly to equation (A54). With only a single scatter placed at origin, the generalized magnetic zeta functions for various boundary conditions in x -direction thus all have the form of

$$\begin{aligned} \mathcal{M}_B^{(k_y e_y, 2D)}(\mathbf{0}, \mathbf{0}; \varepsilon) &= -\frac{4}{2\mu} \frac{1}{L} \sum_{p_y = \frac{2\pi n_y}{L} + k_y, n_y \in \mathbb{Z}} G_B^{(1D)}\left(\frac{p_y}{qB}, \frac{p_y}{qB}; \varepsilon\right) \\ &+ \frac{1}{\pi} \left(2\gamma_E + \ln \frac{\mu\varepsilon\rho^2}{2}\right) \Big|_{\rho \rightarrow 0}. \end{aligned} \quad (24)$$

2.2.1. *Generalized magnetic zeta function for open boundary condition in x-direction.* The generalized magnetic zeta functions for open boundary condition in x-direction is thus explicitly given by

$$\begin{aligned} \mathcal{M}_B^{(\text{Open}, k_y e_y, 2D)}(\mathbf{0}, \mathbf{0}; \varepsilon) &= 4 \frac{\Gamma\left(\frac{1}{2} - \frac{\mu\varepsilon}{qB}\right)}{\sqrt{2qB}\sqrt{2\pi}} \frac{1}{L} \sum_{p_y = \frac{2\pi n_y}{L} + k_y, n_y \in \mathbb{Z}} \\ &\times U\left(-\frac{\mu\varepsilon}{qB}, -\sqrt{2qB} \frac{p_y}{qB}\right) U\left(-\frac{\mu\varepsilon}{qB}, \sqrt{2qB} \frac{p_y}{qB}\right) \\ &+ \frac{1}{\pi} \left(2\gamma_E + \ln \frac{\mu\varepsilon\rho^2}{2}\right) \Big|_{\rho \rightarrow 0}. \end{aligned} \quad (25)$$

The infinite momentum sum in equation (25) is UV divergent that is cancelled out by UV divergent part in the second term. The UV cancellation can be made explicitly by using Kummer function representation of infinite volume magnetic Green's function and equation (25), thus we find

$$\begin{aligned} \mathcal{M}_B^{(\text{Open}, k_y e_y, 2D)}(\mathbf{0}, \mathbf{0}; \varepsilon) &= \mathcal{M}_B^{(\infty, 2D)}(\mathbf{0}, \mathbf{0}; \varepsilon) \\ &+ \frac{1}{\pi} \sum_{n_y \neq 0} e^{-ik_y n_y L} e^{-\frac{qB}{4} |n_y L e_y|^2} \\ &\times \Gamma\left(\frac{1}{2} - \frac{\mu\varepsilon}{qB}\right) U\left(\frac{1}{2} - \frac{\mu\varepsilon}{qB}, 1, \frac{qB}{2} |n_y L e_y|^2\right), \end{aligned} \quad (26)$$

where $\mathcal{M}_B^{(\infty, 2D)}$ is defined in equation (A58).

2.2.2. *Generalized magnetic zeta function for half open boundary condition in x-direction.* For half open boundary condition in x-direction, the UV divergence in infinite momentum sum can be regularized by subtracting by $\mathcal{M}_B^{(\text{Open}, k_y, 2D)}$, thus we find,

$$\begin{aligned} \mathcal{M}_B^{(\text{Half}, k_y e_y, 2D)}(\mathbf{0}, \mathbf{0}; \varepsilon) &= \mathcal{M}_B^{(\text{Open}, k_y e_y, 2D)}(\mathbf{0}, \mathbf{0}; \varepsilon) - \frac{4}{2\mu} \frac{1}{L} \sum_{p_y = \frac{2\pi n_y}{L} + k_y, n_y \in \mathbb{Z}} \\ &\times \left[G_B^{(\text{Half}, 1D)}\left(\frac{p_y}{qB}, \frac{p_y}{qB}; \varepsilon\right) - G_B^{(\text{Open}, 1D)}\left(\frac{p_y}{qB}, \frac{p_y}{qB}; \varepsilon\right) \right]. \end{aligned} \quad (27)$$

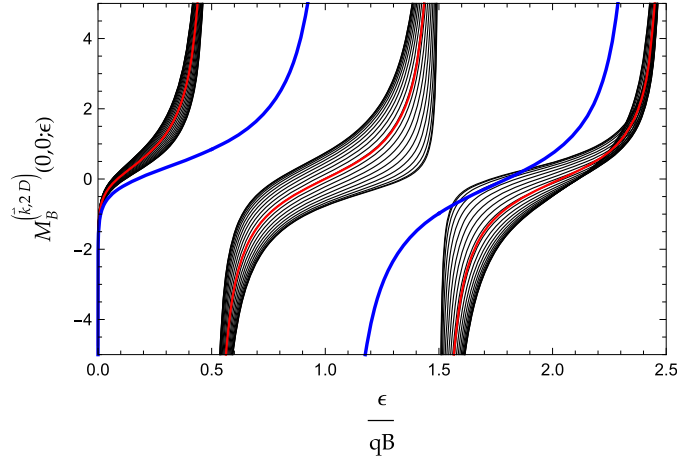


Figure 1. Bulk energy bands (filled with black curves) in finite volume with magnetic periodic boundary condition in both x - and y -direction is generated by varying k_x in magnetic Brillouin zone: $k_x \in [0, \frac{2\pi}{n_q L}]$ in finite volume magnetic zeta function $\mathcal{M}_B^{(L,\mathbf{k},2D)}(\mathbf{0}, \mathbf{0}; \epsilon)$ defined in equation (A54). The wave vector in y -direction, k_y , is fixed at $k_y = \frac{\pi}{2n_q L}$. Compared with $\mathcal{M}_B^{(\text{Open},k_y,2D)}(\mathbf{0}, \mathbf{0}; \epsilon)$ in equation (26) (red curve) with open boundary condition along x -direction and $\mathcal{M}_B^{(\text{h.w.},k_y,2D)}(\mathbf{0}, \mathbf{0}; \epsilon)$ in equation (28) (blue curve) with a hard wall boundary condition in x -direction. The parameters are chosen as: $L = 5$, and $n_q = n_p = 1$.

2.2.3. Generalized magnetic zeta function for hard wall boundary condition in x -direction. Similarly, for hard wall boundary condition in x -direction, by subtracting with $\mathcal{M}_B^{(\text{Open},k_y,2D)}$, the UV regularized magnetic zeta function is given by

$$\begin{aligned} & \mathcal{M}_B^{(\text{h.w.},k_y,2D)}(\mathbf{0}, \mathbf{0}; \epsilon) \\ &= \mathcal{M}_B^{(\text{Open},k_y,2D)}(\mathbf{0}, \mathbf{0}; \epsilon) - \frac{4}{2\mu L} \sum_{p_y = \frac{2\pi n_y}{L} + k_y, n_y \in \mathbb{Z}} \\ & \times \left[G_B^{(\text{h.w.},1D)}\left(\frac{p_y}{qB}, \frac{p_y}{qB}; \epsilon\right) - G_B^{(\text{Open},1D)}\left(\frac{p_y}{qB}, \frac{p_y}{qB}; \epsilon\right) \right]. \end{aligned} \quad (28)$$

2.3. Energy spectrum of edge states vs bulk energy bands

The bulk states are related to the periodic boundary condition solutions in both directions. In LQCD, CM momenta of two particles, \mathbf{P}_B , become discrete due to the constraints of periodic boundary condition. Hence it also yields discrete energy spectra. When discrete total momentum \mathbf{P}_B or $\mathbf{k} = \frac{\mathbf{P}_B}{2}$ is varied continuously, also see detailed discussion in appendix B, the discrete energy spectra are smeared into isolated bulk energy bands. For a topological trivial system, these bands are separated by forbidden gaps due to particles interaction. On the contrary, for a non-trivial topological system, such as a magnetic system, the non-trivial topological edge states show up in forbidden gaps when periodic boundary condition is replaced by Dirichlet boundary condition. Hence the isolated energy bands can be connected continuously and smoothly by topological edge states. When \mathbf{k} is further taken into a complex plane, the

real solutions in the gaps can also be found that provides an alternative way of crossing over gap and connecting two isolated bands smoothly. The discussion of analytic continuation of solutions in forbidden gaps can be found in appendix C.

For periodic boundary conditions in both x - and y -direction, with a fixed k_y , the bulk energy bands can be generated by treating k_x as a free parameter in finite volume magnetic zeta function $\mathcal{M}_B^{(L,k,2D)}(\mathbf{0}, \mathbf{0}; \varepsilon)$ that is defined in equation (A54), see figure 1. The bulk energy bands are separated by gaps in between. The edge states are produced by replacing the periodic boundary condition in x -direction by a hard wall boundary condition, $\mathcal{M}_B^{(h.w.,k_y,2D)}(\mathbf{0}, \mathbf{0}; \varepsilon)$ in equation (28). As shown in figure 1, unlike topologically trivial edge states, the solutions of edge states of a magnetic system not only show up in the gap, but also punch through bulk energy bands.

3. Summary

In summary, the formalism of a finite volume magnetic two-hadron system with Dirichlet boundary condition in one spatial direction is derived, and quantization condition under the assumption of contact interaction potential is obtained and presented in current work. The formalism may be useful in the future lattice study of magnetic polarizability of hadron resonances, and also it may be useful for the study of phase structure of QCD, such as, how the magnetic field may turn charged hadron resonances massless and vacuum into a superconductor, etc.

Acknowledgments

We acknowledge support from the Department of Physics and Engineering, California State University, Bakersfield, CA.

Data availability statement

All data that support the findings of this study are included within the article (and any supplementary files).

Appendix A. Finite volume dynamics of a magnetic system in a plane

The dynamics of relative motion of two-particle system in a uniform magnetic field is described by the finite volume Lippmann–Schwinger (LS) equation,

$$\psi_\varepsilon^{(L, \frac{\mathbf{P}_B}{2})}(\mathbf{r}) = \int_{L_B^3} d\mathbf{r}' G_B^{(L, \frac{\mathbf{P}_B}{2})}(\mathbf{r}, \mathbf{r}'; \varepsilon) V^{(L)}(\mathbf{r}') \psi_\varepsilon^{(L, \frac{\mathbf{P}_B}{2})}(\mathbf{r}'), \quad (\text{A1})$$

where the volume integration over the enlarged magnetic unit cell,

$$n_q L \mathbf{e}_x \times L \mathbf{e}_y \times L \mathbf{e}_z,$$

is defined by

$$\int_{L_B^3} d\mathbf{r}' = \int_{-\frac{n_q L}{2}}^{\frac{n_q L}{2}} dr'_x \int_{-\frac{L}{2}}^{\frac{L}{2}} dr'_y \int_{-\frac{L}{2}}^{\frac{L}{2}} dr'_z. \quad (\text{A2})$$

The wavefunction satisfies the magnetic periodic boundary condition,

$$\psi_\varepsilon^{(L, \frac{\mathbf{P}_B}{2})}(\mathbf{r} + \mathbf{n}_B L) = e^{i \frac{\mathbf{P}_B}{2} \cdot \mathbf{n}_B L} e^{-iq B r_y \mathbf{e}_x \cdot \mathbf{n}_B L} \psi_\varepsilon^{(L, \frac{\mathbf{P}_B}{2})}(\mathbf{r}), \quad (\text{A3})$$

where

$$\mathbf{n}_B = n_x n_q \mathbf{e}_x + n_y \mathbf{e}_y + n_z \mathbf{e}_z, \quad n_{x,y,z} \in \mathbb{Z}, \quad (\text{A4})$$

and

$$\mathbf{P}_B = \frac{2\pi}{L} \left(\frac{n_x}{n_q} \mathbf{e}_x + n_y \mathbf{e}_y + n_z \mathbf{e}_z \right), \quad n_{x,y,z} \in \mathbb{Z}. \quad (\text{A5})$$

The finite volume magnetic Green's function $G_B^{(L, \frac{\mathbf{P}_B}{2})}$ satisfies equation,

$$(\varepsilon - \hat{H}_r) G_B^{(L, \frac{\mathbf{P}_B}{2})}(\mathbf{r}, \mathbf{r}'; \varepsilon) = \sum_{\mathbf{n}_B} e^{-i \frac{\mathbf{P}_B}{2} \cdot \mathbf{n}_B L} e^{iq B r_y \mathbf{e}_x \cdot \mathbf{n}_B L} \delta(\mathbf{r} - \mathbf{r}' + \mathbf{n}_B L), \quad (\text{A6})$$

where the Hamiltonian of relative motion of two charged particles in a uniform magnetic field is given by

$$\hat{H}_r = -\frac{(\nabla_r + iq \mathbf{A}(\mathbf{r}))^2}{2\mu}. \quad (\text{A7})$$

q and μ stand for effective charge and mass of two particles respectively. The uniform magnetic field is chosen along z -axis, $\mathbf{B} = B \mathbf{e}_z$, and Landau gauge for vector potential is adopted in this work,

$$\mathbf{A}(\mathbf{x}) = B(0, x, 0). \quad (\text{A8})$$

To warrant a state that is translated through a closed path remain same, the magnetic flux $q B n_q L^2$ through the surface of an enlarged magnetic unit cell in x - y plane must be quantized:

$$q B n_q L^2 = 2\pi n_p, \quad (\text{A9})$$

where n_p and n_q are two relatively prime integers.

The analytic solutions of $G_B^{(L, \frac{\mathbf{P}_B}{2})}$ can be constructed from its infinite volume counterpart $G_B^{(\infty)}$ by,

$$\begin{aligned} G_B^{(L, \frac{\mathbf{P}_B}{2})}(\mathbf{r}, \mathbf{r}'; \varepsilon) &= \sum_{\mathbf{n}_B} G_B^{(\infty)}(\mathbf{r}, \mathbf{r}' + \mathbf{n}_B L; \varepsilon) e^{i \frac{\mathbf{P}_B}{2} \cdot \mathbf{n}_B L} e^{-iq B r'_y \mathbf{e}_x \cdot \mathbf{n}_B L} \\ &= \sum_{\mathbf{n}_B} e^{-i \frac{\mathbf{P}_B}{2} \cdot \mathbf{n}_B L} e^{iq B r_y \mathbf{e}_x \cdot \mathbf{n}_B L} G_B^{(\infty)}(\mathbf{r} + \mathbf{n}_B L, \mathbf{r}'; \varepsilon), \end{aligned} \quad (\text{A10})$$

where the infinite volume magnetic Green's function $G_B^{(\infty)}$ satisfies equation,

$$(\varepsilon - \hat{H}_r) G_B^{(\infty)}(\mathbf{r}, \mathbf{r}'; \varepsilon) = \delta(\mathbf{r} - \mathbf{r}'). \quad (\text{A11})$$

The 3D analytic expression of $G_B^{(\infty)}$ is related to 2D magnetic Green's function that is defined in x - y plane, $G_B^{(\infty,2D)}$, by

$$G_B^{(\infty)}(\mathbf{r}, \mathbf{r}'; \varepsilon) = \int_{-\infty}^{\infty} \frac{dp_z}{2\pi} G_B^{(\infty,2D)}\left(\boldsymbol{\rho}, \boldsymbol{\rho}'; \varepsilon - \frac{p_z^2}{2\mu}\right) e^{ip_z(r_z - r'_z)}, \quad (\text{A12})$$

where

$$\boldsymbol{\rho} = r_x \mathbf{e}_x + r_y \mathbf{e}_y, \quad \boldsymbol{\rho}' = r'_x \mathbf{e}_x + r'_y \mathbf{e}_y$$

are relative coordinates defined in x - y plane. The various representations of 2D infinite volume magnetic Green's function, $G_B^{(\infty,2D)}$, are given by

$$\begin{aligned} G_B^{(\infty,2D)}(\boldsymbol{\rho}, \boldsymbol{\rho}'; \varepsilon) &= \sum_{n=0}^{\infty} \int_{-\infty}^{\infty} \frac{dp_y}{2\pi} \frac{\phi_n\left(r_x + \frac{p_y}{qB}\right) \phi_n^*\left(r'_x + \frac{p_y}{qB}\right) e^{ip_y(r_y - r'_y)}}{\varepsilon - \frac{qB}{\mu}\left(n + \frac{1}{2}\right)} \\ &= \frac{qB}{2\pi} e^{-\frac{iqB}{2}(r_x + r'_x)(r_y - r'_y)} \sum_{n=0}^{\infty} \frac{L_n\left(\frac{qB}{2}|\boldsymbol{\rho} - \boldsymbol{\rho}'|^2\right) e^{-\frac{qB}{4}|\boldsymbol{\rho} - \boldsymbol{\rho}'|^2}}{\varepsilon - \frac{qB}{\mu}\left(n + \frac{1}{2}\right)} \\ &= -\frac{2\mu}{4\pi} e^{-\frac{iqB}{2}(r_x + r'_x)(r_y - r'_y)} e^{-\frac{qB}{4}|\boldsymbol{\rho} - \boldsymbol{\rho}'|^2} \Gamma\left(\frac{1}{2} - \frac{\mu\varepsilon}{qB}\right) \\ &\quad \times U\left(\frac{1}{2} - \frac{\mu\varepsilon}{qB}, 1, \frac{qB}{2}|\boldsymbol{\rho} - \boldsymbol{\rho}'|^2\right), \end{aligned} \quad (\text{A13})$$

where $\phi_n(r_x)$ is eigen-solution of 1D harmonic oscillator potential,

$$\phi_n(r_x) = \frac{1}{\sqrt{2^n n!}} \left(\frac{qB}{\pi}\right)^{\frac{1}{4}} e^{-\frac{qB}{2}r_x^2} H_n(\sqrt{qB}r_x). \quad (\text{A14})$$

$H_n(x)$, $L_n(x)$ and $U(a, b, z)$ are standard Hermite polynomial, Laguerre polynomial and Kummer function respectively [78].

From this point on, all the discussions will be restricted in x - y plane, the purpose of this is only to simplify the technical presentations. The conclusions can in principle be extended into 3D as well by using relation in equation (A12). In this section, the dynamical equations of a magnetic system in a plane will be reformulated in terms of new basis functions that satisfy magnetic periodic boundary conditions. In terms of these magnetic periodic basis functions, reaction amplitudes may be introduced, and LS equation of reaction amplitudes is thus obtained. The relation to Harper's equation is presented when a specific type of potential is considered. At last, the quantization conditions in 2D plane with contact interactions are presented and discussed.

In x - y plane, similar to equation (A1), the finite volume LS equation in 2D is given by

$$\psi_{\varepsilon}^{(L, \frac{P_B}{2}, 2D)}(\boldsymbol{\rho}) = \int_{L_B^2} d\boldsymbol{\rho}' G_B^{(L, \frac{P_B}{2}, 2D)}(\boldsymbol{\rho}, \boldsymbol{\rho}'; \varepsilon) V^{(L)}(\boldsymbol{\rho}') \psi_{\varepsilon}^{(L, \frac{P_B}{2}, 2D)}(\boldsymbol{\rho}'), \quad (\text{A15})$$

where the volume integration over the magnetic unit cell is defined by

$$\int_{L_B^2} d\boldsymbol{\rho}' = \int_{-\frac{nqL}{2}}^{\frac{nqL}{2}} dr'_x \int_{-\frac{L}{2}}^{\frac{L}{2}} dr'_y. \quad (\text{A16})$$

One of analytic expression of finite volume 2D magnetic Green's function is explicitly given by

$$\begin{aligned}
 &G_B^{(L, \frac{\mathbf{P}_B}{2}, 2D)}(\boldsymbol{\rho}, \boldsymbol{\rho}'; \varepsilon) \\
 &= \sum_{n=0}^{\infty} \sum_{n_x \in \mathbb{Z}} e^{-i(\frac{P_{Bx}}{2} - qBr_y)n_x n_q L} \frac{1}{L} \sum_{p_y = \frac{2\pi n_y}{L} + \frac{P_{By}}{2}, n_y \in \mathbb{Z}} \\
 &\quad \times \frac{\phi_n\left(r_x + n_x n_q L + \frac{P_y}{qB}\right) \phi_n^*\left(r'_x + \frac{P_y}{qB}\right) e^{ip_y(r_y - r'_y)}}{\varepsilon - \frac{qB}{\mu}\left(n + \frac{1}{2}\right)}. \tag{A17}
 \end{aligned}$$

By splitting lattice sum of n_y in k_y in equation (A17) using identity,

$$\sum_{n_y \in \mathbb{Z}} f(n_y) = \sum_{\alpha=0}^{n_p-1} \sum_{\bar{n}_y \in \mathbb{Z}} f(n_p \bar{n}_y + \alpha), \tag{A18}$$

and also performing a shifting in lattice sum of $n_x: n_x \rightarrow n_x - \bar{n}_y$, the finite volume 2D magnetic Green's function thus can also be written as

$$G_B^{(L, \frac{\mathbf{P}_B}{2}, 2D)}(\boldsymbol{\rho}, \boldsymbol{\rho}'; \varepsilon) = \sum_{n=0}^{\infty} \sum_{\alpha=0}^{n_p-1} \frac{\chi_{n,\alpha}^{(\frac{\mathbf{P}_B}{2})}(\boldsymbol{\rho}) \chi_{n,\alpha}^{(\frac{\mathbf{P}_B}{2})^*}(\boldsymbol{\rho}')}{\varepsilon - \frac{qB}{\mu}\left(n + \frac{1}{2}\right)}, \tag{A19}$$

where

$$\begin{aligned}
 \chi_{n,\alpha}^{(\frac{\mathbf{P}_B}{2})}(\boldsymbol{\rho}) &= \frac{1}{\sqrt{L}} \sum_{n_x \in \mathbb{Z}} \phi_n\left(r_x + \frac{2\pi(n_p n_x + \alpha)}{L} + \frac{P_{By}}{2}\right) e^{-i\frac{P_{Bx}}{2} n_x n_q L} \\
 &\quad \times e^{i\left(\frac{2\pi(n_p n_x + \alpha)}{L} + \frac{P_{By}}{2}\right) r_y}. \tag{A20}
 \end{aligned}$$

The $\chi_{n,\alpha}^{(\frac{\mathbf{P}_B}{2})}(\boldsymbol{\rho})$ functions are solutions of Schrödinger equation with degeneracy of n_p for a fixed n value,

$$\begin{aligned}
 &\left(\frac{qB}{\mu}\left(n + \frac{1}{2}\right) - \hat{H}_\rho\right) \chi_{n,\alpha}^{(\frac{\mathbf{P}_B}{2})}(\boldsymbol{\rho}) = 0, \tag{A21} \\
 &\alpha = 0, 1, \dots, n_p - 1,
 \end{aligned}$$

and they too satisfy magnetic periodic boundary condition,

$$\chi_{n,\alpha}^{(\frac{\mathbf{P}_B}{2})}(\boldsymbol{\rho} + \mathbf{n}_B L) = e^{i\frac{\mathbf{P}_B}{2} \cdot \mathbf{n}_B L} e^{-iqBr_y} e^{i\mathbf{n}_B L} \chi_{n,\alpha}^{(\frac{\mathbf{P}_B}{2})}(\boldsymbol{\rho}). \tag{A22}$$

Using orthogonality relation of 1D harmonic oscillator basis functions,

$$\int_{-\infty}^{\infty} dr_x \phi_n(r_x) \phi_{n'}^*(r_x) = \delta_{n,n'}, \tag{A23}$$

and also completeness of 1D harmonic oscillator basis

$$\sum_{n=0}^{\infty} \phi_n(r_x) \phi_n^*(r'_x) = \delta(r_x - r'_x), \tag{A24}$$

one can show easily that $\chi_{n,\alpha}^{(\mathbf{P}_B)}(\boldsymbol{\rho})$ functions are orthogonal,

$$\int_{L_B^2} d\boldsymbol{\rho} \chi_{n,\alpha}^{(\mathbf{P}_B)}(\boldsymbol{\rho}) \chi_{n',\alpha'}^{(\mathbf{P}_B)*}(\boldsymbol{\rho}) = \delta_{\alpha,\alpha'} \delta_{n,n'}, \tag{A25}$$

and form a complete magnetic periodic basis as well,

$$\begin{aligned} & \sum_{n=0}^{\infty} \sum_{\alpha=0}^{n_p-1} \chi_{n,\alpha}^{(\mathbf{P}_B)}(\boldsymbol{\rho}) \chi_{n,\alpha}^{(\mathbf{P}_B)*}(\boldsymbol{\rho}') \\ &= \sum_{\mathbf{n}_B} e^{-i\frac{\mathbf{P}_B}{2} \cdot \mathbf{n}_B L} e^{iqB r_{\gamma} \mathbf{e}_x \cdot \mathbf{n}_B L} \delta(\boldsymbol{\rho} - \boldsymbol{\rho}' + \mathbf{n}_B L). \end{aligned} \tag{A26}$$

Therefore, in presence of magnetic field, it is more convenient to use $\chi_{n,\alpha}^{(\mathbf{P}_B)}(\boldsymbol{\rho})$ as basis functions instead of plane wave, such as $e^{i\mathbf{k} \cdot \boldsymbol{\rho}}$ with $\mathbf{k} = \frac{2\pi\mathbf{n}}{L} + \frac{\mathbf{P}}{2}$ and $\mathbf{n} \in \mathbb{Z}^2$, which are common choice in finite volume.

A.1. Finite volume reaction amplitudes of a magnetic system

In absence of magnetic field, the momentum representation of finite volume LS equation normally has the form of

$$T_{\mathbf{P}}^{(\frac{\mathbf{P}}{2})}(\varepsilon) = \frac{1}{L^2} \sum_{\mathbf{P}'} \frac{\tilde{V}_{\mathbf{P},\mathbf{P}'}}{\varepsilon - \frac{\mathbf{P}'^2}{2\mu}} T_{\mathbf{P}'}^{(\frac{\mathbf{P}}{2})}(\varepsilon), \tag{A27}$$

where

$$(\mathbf{P}, \mathbf{P}') \in \frac{2\pi\mathbf{n}}{L} + \frac{\mathbf{P}}{2}, \quad \mathbf{n} \in \mathbb{Z}^2,$$

and $\mathbf{P} = \frac{2\pi\mathbf{d}}{L}$, $\mathbf{d} \in \mathbb{Z}^2$ represents the total momentum of particles system. The finite volume scattering amplitude $T_{\mathbf{P}}^{(\frac{\mathbf{P}}{2})}(\varepsilon)$ amplitudes and matrix element of potential are defined in terms of plane wave basis by

$$\begin{aligned} T_{\mathbf{P}}^{(\frac{\mathbf{P}}{2})}(\varepsilon) &= - \int_{L^2} d\boldsymbol{\rho}' e^{-i\mathbf{P} \cdot \boldsymbol{\rho}'} V^{(L)}(\boldsymbol{\rho}') \psi_{\varepsilon}^{(L, \frac{\mathbf{P}}{2}, 2D)}(\boldsymbol{\rho}'), \\ \tilde{V}_{\mathbf{P},\mathbf{P}'} &= \int_{L^2} d\boldsymbol{\rho} e^{-i\mathbf{P} \cdot \boldsymbol{\rho}} V^{(L)}(\boldsymbol{\rho}) e^{i\mathbf{P}' \cdot \boldsymbol{\rho}}, \end{aligned} \tag{A28}$$

see e.g. reference [25].

Similarly, with the magnetic field on, the finite volume reaction amplitude may be introduced in terms of $\chi_{n,\alpha}^{(\mathbf{P}_B)}(\boldsymbol{\rho})$ basis functions by

$$T_{n,\alpha}^{(\mathbf{P}_B)}(\varepsilon) = - \int_{L_B^2} d\boldsymbol{\rho}' \chi_{n,\alpha}^{(\mathbf{P}_B)*}(\boldsymbol{\rho}') V^{(L)}(\boldsymbol{\rho}') \psi_{\varepsilon}^{(L, \mathbf{P}_B, 2D)}(\boldsymbol{\rho}'). \tag{A29}$$

Using equation (A19), the representation of LS equation (A15) in terms of finite volume reaction amplitudes is thus obtained

$$T_{n,\alpha}^{(\frac{P_B}{2})}(\varepsilon) = \sum_{n'=0}^{\infty} \sum_{\alpha'=0}^{n_p-1} \frac{V_{n,\alpha;n',\alpha'}^{(\frac{P_B}{2})}}{\varepsilon - \frac{qB}{\mu} (n' + \frac{1}{2})} T_{n',\alpha'}^{(\frac{P_B}{2})}(\varepsilon), \tag{A30}$$

where

$$V_{n,\alpha;n',\alpha'}^{(\frac{P_B}{2})} = \int_{L_B^2} d\rho \chi_{n,\alpha}^{(\frac{P_B}{2})*}(\rho) V^{(L)}(\rho) \chi_{n',\alpha'}^{(\frac{P_B}{2})}(\rho). \tag{A31}$$

Hence, the energy spectrum of a magnetic system may be determined from homogenous equation, equation (A30), by

$$\det \left[\delta_{n,\alpha;n',\alpha'} - \frac{V_{n,\alpha;n',\alpha'}^{(\frac{P_B}{2})}}{\varepsilon - \frac{qB}{\mu} (n' + \frac{1}{2})} \right] = 0. \tag{A32}$$

A.2. Relation to Harper's equation

In this subsection, we will show how the well-known Harper's equation [82, 88] is obtained from equation (A30), when a specific type of potential is considered,

$$V^{(L)}(\rho) = V_1 \cos \frac{2\pi r_x}{L} + V_2 \cos \frac{2\pi r_y}{L}. \tag{A33}$$

Thus, the matrix element of potential term is given by

$$V_{n,\alpha;n',\alpha'}^{(\frac{P_B}{2})} = \delta_{\alpha,\alpha'} \frac{e^{-i\frac{2\pi\alpha + \frac{P_{By}}{2}}{\frac{L}{2\pi}qB}} + (-1)^{n+n'} e^{i\frac{2\pi\alpha + \frac{P_{By}}{2}}{\frac{L}{2\pi}qB}}}{2} V_{n,n'}^{(1)} + \frac{\delta_{\alpha,\alpha'+1} V_{n,n'}^{(2,-)} + \delta_{\alpha,\alpha'-1} V_{n,n'}^{(2,+)}}{2}, \tag{A34}$$

where

$$V_{n,n'}^{(1)} = V_1 \int_{-\infty}^{\infty} dr_x \phi_n^*(r_x) e^{i\frac{2\pi r_x}{L}} \phi_{n'}(r_x), \tag{A35}$$

$$V_{n,n'}^{(2,\pm)} = V_2 \int_{-\infty}^{\infty} dr_x \phi_n^* \left(r_x \pm \frac{1}{\frac{L}{2\pi}qB} \right) \phi_{n'}(r_x).$$

Redefining reaction amplitude by

$$T_{n,\alpha}^{(\frac{P_B}{2})}(\varepsilon) = \left(\varepsilon - \frac{qB}{\mu} \left(n + \frac{1}{2} \right) \right) d_{n,\alpha}^{(\frac{P_B}{2})}(\varepsilon) e^{i\frac{P_{Bx}}{2} \frac{2\pi\alpha}{qB}}, \tag{A36}$$

and also adopting nearest neighbour approximation:

$$V_{n,n'}^{(1)} \simeq \delta_{n,n'} V_n^{(1)}, \quad V_{n,n'}^{(2,\pm)} \simeq \delta_{n,n'} V_n^{(2)}, \tag{A37}$$

the LS equation (A30) can thus be turned into Harper's equation [82, 88],

$$\begin{aligned} & \left(\varepsilon - \frac{qB}{\mu} \left(n + \frac{1}{2} \right) \right) d_{n,\alpha}^{(\frac{P_B}{2})}(\varepsilon) \\ &= V_n^{(1)} \cos \left(\frac{\frac{2\pi\alpha}{L} + \frac{P_{By}}{2}}{\frac{L}{2\pi}qB} \right) d_{n,\alpha}^{(\frac{P_B}{2})}(\varepsilon) \\ &+ \frac{V_n^{(2)}(\varepsilon) e^{-i\frac{P_{Bx}}{2}qB} d_{n,\alpha-1}^{(\frac{P_B}{2})} + e^{i\frac{P_{Bx}}{2}qB} d_{n,\alpha+1}^{(\frac{P_B}{2})}(\varepsilon)}{2}. \end{aligned} \tag{A38}$$

The Harper's equation plays a crucial role in understanding topological features of a magnetic system in condensed matter physics, see e.g. [82].

A.3. Contact interaction and quantization condition

The short-range nuclear force may be modeled by contact interaction, in this work, S -wave dominance is assumed, so we will adopt a simple periodic contact potential,

$$V^{(L)}(\boldsymbol{\rho}) = \sum_{\mathbf{n} \in \mathbb{Z}^2} V_0 \delta(\boldsymbol{\rho} + \mathbf{n}L). \tag{A39}$$

Hence equation (A1) is reduced to matrix equation,

$$\begin{aligned} & \psi_\varepsilon^{(L, \frac{P_B}{2}, 2D)}(\eta \mathbf{L} \mathbf{e}_x) \\ &= \sum_{\eta'=0}^{n_q-1} G_B^{(L, \frac{P_B}{2}, 2D)}(\eta \mathbf{L} \mathbf{e}_x, \eta' \mathbf{L} \mathbf{e}_x; \varepsilon) V_0 \psi_\varepsilon^{(L, \frac{P_B}{2}, 2D)}(\eta' \mathbf{L} \mathbf{e}_x), \end{aligned} \tag{A40}$$

where $\eta = 0, \dots, n_q - 1$, and $\eta \mathbf{e}_x$ stand for the location of n_q scattering centers placed in an enlarged magnetic cell in a plane: $n_q \mathbf{L} \mathbf{e}_x \times \mathbf{L} \mathbf{e}_y$. The eigen-energy spectrum is thus determined by quantization condition,

$$\det \left[\frac{\delta_{\eta, \eta'}}{V_0} - G_B^{(L, \frac{P_B}{2}, 2D)}(\eta \mathbf{L} \mathbf{e}_x, \eta' \mathbf{L} \mathbf{e}_x; \varepsilon) \right] = 0. \tag{A41}$$

Both bare strength of potential V_0 and the diagonal component of finite volume magnetic Green's function, $G_B^{(L, \frac{P_B}{2}, 2D)}$, are ultra-violet (UV) divergent. Ultimately, UV divergence in both V_0 and $G_B^{(L, \frac{P_B}{2}, 2D)}$ must be regularized and cancel out explicitly, and quantization condition in equation (A41) is thus free of UV divergence and well-defined.

A.3.1. Scattering in infinite volume with a contact interaction. In a infinite 2D plane, the two-body scattering by a contact interaction,

$$V^{(\infty)}(\boldsymbol{\rho}) = V_0 \delta(\boldsymbol{\rho}), \tag{A42}$$

is described by a inhomogeneous LS equation,

$$\psi_{\mathbf{k}}^{(\infty, 2D)}(\boldsymbol{\rho}) = e^{i\mathbf{k} \cdot \boldsymbol{\rho}} + V_0 G_0^{(\infty, 2D)}(\boldsymbol{\rho}; \varepsilon) \psi_{\mathbf{k}}^{(\infty, 2D)}(\mathbf{0}), \tag{A43}$$

where \mathbf{k} stands for incoming relative momentum of two particles, and it is related to ε by

$$k^2 = 2\mu\varepsilon.$$

The infinite volume Green's function is given by

$$G_0^{(\infty,2D)}(\boldsymbol{\rho}; \varepsilon) = \int_{-\infty}^{\infty} \frac{d\mathbf{p}}{(2\pi)^2} \frac{e^{i\mathbf{p}\cdot\boldsymbol{\rho}}}{\varepsilon - \frac{\mathbf{p}^2}{2\mu}} = -\frac{2\mu i}{4} H_0^{(1)}(k\rho). \tag{A44}$$

The equation (A43) can be rewritten as

$$\psi_{\mathbf{k}}^{(\infty,2D)}(\boldsymbol{\rho}) = e^{i\mathbf{k}\cdot\boldsymbol{\rho}} + i t_0^{(\infty)}(k) H_0^{(1)}(k\rho), \tag{A45}$$

where

$$t_0^{(\infty)}(k) = -\frac{2\mu}{4} \frac{1}{\frac{1}{V_0} - G_0^{(\infty,2D)}(\mathbf{0}; \varepsilon)} \tag{A46}$$

represents S -wave two-body scattering amplitude. $t_0^{(\infty)}(k)$ is normally parameterized by a phase shift,

$$t_0^{(\infty)}(k) = \frac{1}{\cot \delta_0(\varepsilon) - i}. \tag{A47}$$

Hence, V_0 is related to scattering phase shift in infinite volume by

$$\cot \delta_0(\varepsilon) = -\frac{4}{2\mu V_0} + \frac{2}{\pi} \left(\gamma_E + \frac{1}{2} \ln \frac{\mu\varepsilon\rho^2}{2} \right) \Big|_{\rho \rightarrow 0}. \tag{A48}$$

A.3.2. Quantization condition of a magnetic system in infinite volume. The eigen-energy of the charge particles system in a uniform magnetic field is in fact discretized even in infinite volume. The dynamics of a trapped system by magnetic field in infinite volume is also described by a homogeneous equation similar to equation (A1). Hence, with a contact interaction given in equation (A42), the quantization condition of a magnetic system in infinite volume is thus given by

$$\frac{1}{V_0} = G_B^{(\infty,2D)}(\mathbf{0}, \mathbf{0}; \varepsilon), \tag{A49}$$

where

$$G_B^{(\infty,2D)}(\mathbf{0}, \mathbf{0}; \varepsilon) = -\frac{2\mu}{4\pi} \Gamma \left(\frac{1}{2} - \frac{\mu\varepsilon}{qB} \right) U \left(\frac{1}{2} - \frac{\mu\varepsilon}{qB}, 1, \frac{qB}{2} \rho^2 \right) \Big|_{\rho \rightarrow 0}. \tag{A50}$$

Using equation (A48) and asymptotic form of Kummer function,

$$\begin{aligned} -\Gamma \left(\frac{1}{2} - \frac{\mu\varepsilon}{qB} \right) U \left(\frac{1}{2} - \frac{\mu\varepsilon}{qB}, 1, \frac{qB}{2} \rho^2 \right) \Big|_{\rho \rightarrow 0} &= 2\gamma_E + \psi \left(\frac{1}{2} - \frac{\mu\varepsilon}{qB} \right) \\ &+ \ln \frac{qB\rho^2}{2} \Big|_{\rho \rightarrow 0}, \end{aligned} \tag{A51}$$

where

$$\psi(x) = \frac{d}{dx} \ln \Gamma(x)$$

is logarithmic derivative of the Gamma function, thus, after UV cancellation, we find

$$\cot \delta_0(\varepsilon) - \mathcal{M}_B^{(\infty, 2D)}(\mathbf{0}, \mathbf{0}; \varepsilon) = 0, \quad (\text{A52})$$

where

$$\mathcal{M}_B^{(\infty, 2D)}(\mathbf{0}, \mathbf{0}; \varepsilon) = -\frac{1}{\pi} \left[\psi \left(\frac{1}{2} - \frac{\mu\varepsilon}{qB} \right) + \ln \frac{qB}{\mu\varepsilon} \right], \quad (\text{A53})$$

is UV-free and well-defined function in infinite volume.

A.3.3. Quantization condition in finite volume. Using equation (A48) and also introducing the matrix elements of generalized magnetic zeta function by

$$\begin{aligned} \mathcal{M}_B^{(L, \frac{P_B}{2}, 2D)}(\eta \mathbf{L}e_x, \eta' \mathbf{L}e_x; \varepsilon) &= -\frac{4}{2\mu} G_B^{(L, \frac{P_B}{2}, 2D)}(\eta \mathbf{L}e_x, \eta' \mathbf{L}e_x; \varepsilon) \\ &\quad + \delta_{\eta, \eta'} \frac{1}{\pi} \left(\gamma_E + \frac{1}{2} \ln \frac{\mu\varepsilon\rho^2}{2} \right) \Big|_{\rho \rightarrow 0}, \end{aligned} \quad (\text{A54})$$

thus, the quantization condition in equation (A41) now can be recasted in a Lüscher formula-like form [1],

$$\det \left[\delta_{\eta, \eta'} \cot \delta_0(\varepsilon) - \mathcal{M}_B^{(L, \frac{P_B}{2}, 2D)}(\eta \mathbf{L}e_x, \eta' \mathbf{L}e_x; \varepsilon) \right] = 0, \quad (\text{A55})$$

where $(\eta, \eta') = 0, \dots, n_q - 1$.

Using equations (A10) and (A13), the generalized magnetic zeta function is thus given explicitly by

$$\begin{aligned} &\mathcal{M}_B^{(L, \frac{P_B}{2}, 2D)}(\eta \mathbf{L}e_x, \eta' \mathbf{L}e_x; \varepsilon) \\ &= \mathcal{M}_B^{(\infty, 2D)}(\eta \mathbf{L}e_x, \eta' \mathbf{L}e_x; \varepsilon) \\ &\quad + \frac{1}{\pi} \sum_{\mathbf{n}_B \neq \mathbf{0}} e^{-i\frac{P_B}{2} \cdot \mathbf{n}_B L} e^{iqB\eta n_q L^2} \\ &\quad \times e^{-\frac{iqB}{2}(\eta L + \eta' L + n_x n_q L) n_y L} e^{-\frac{qB}{4}|(\eta - \eta')\mathbf{L}e_x + \mathbf{n}_B L|^2} \\ &\quad \times \Gamma \left(\frac{1}{2} - \frac{\mu\varepsilon}{qB} \right) U \left(\frac{1}{2} - \frac{\mu\varepsilon}{qB}, 1, \frac{qB}{2}|(\eta - \eta')\mathbf{L}e_x + \mathbf{n}_B L|^2 \right), \end{aligned} \quad (\text{A56})$$

where

$$\begin{aligned} \mathcal{M}_B^{(\infty, 2D)}(\eta \mathbf{L}e_x, \eta' \mathbf{L}e_x; \varepsilon) &= -\frac{4}{2\mu} G_B^{(\infty, 2D)}(\eta \mathbf{L}e_x, \eta' \mathbf{L}e_x; \varepsilon) \\ &\quad + \delta_{\eta, \eta'} \frac{1}{\pi} \left(\gamma_E + \frac{1}{2} \ln \frac{\mu\varepsilon\rho^2}{2} \right) \Big|_{\rho \rightarrow 0}. \end{aligned} \quad (\text{A57})$$

Only diagonal terms of infinite volume magnetic Green's function, $G_B^{(\infty, 2D)}$, are UV divergent. Using equation (A51) again, thus the UV regularized diagonal terms of $\mathcal{M}_B^{(\infty, 2D)}$ function is

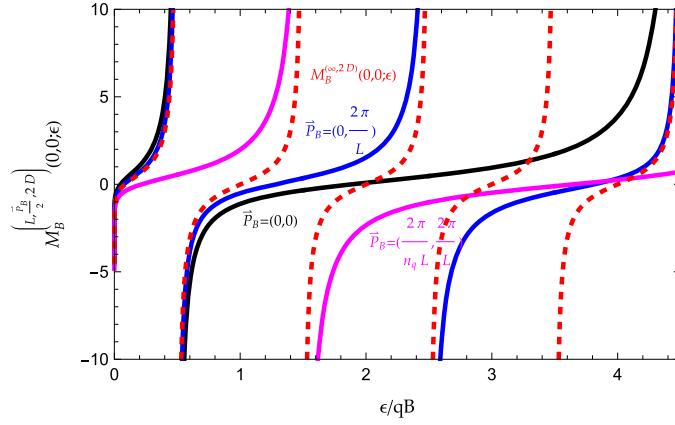


Figure 2. The plot of finite volume magnetic zeta function $\mathcal{M}_B^{(L, \frac{\mathbf{P}_B}{2}, 2D)}(\mathbf{0}, \mathbf{0}; \varepsilon)$ defined in equation (A54) vs $\mathcal{M}_B^{(\infty, 2D)}(\mathbf{0}, \mathbf{0}; \varepsilon)$ (red dashed) given in equation (A58). The solid black, blue and pink curves are corresponding to $\mathbf{P}_B = (0, 0)$, $(0, \frac{2\pi}{L})$ and $(\frac{2\pi}{n_q L}, \frac{2\pi}{L})$ respectively. The parameters are chosen as: $L = 5$, and $n_q = n_p = 1$.

given again by

$$\mathcal{M}_B^{(\infty, 2D)}(\eta L e_x, \eta L e_x; \varepsilon) = -\frac{1}{\pi} \left[\psi \left(\frac{1}{2} - \frac{\mu \varepsilon}{qB} \right) + \ln \frac{qB}{\mu \varepsilon} \right]. \quad (\text{A58})$$

The example plot of $\mathcal{M}_B^{(L, \frac{\mathbf{P}_B}{2}, 2D)}(\mathbf{0}, \mathbf{0}; \varepsilon)$ for various of \mathbf{P}_B 's compared with $\mathcal{M}_B^{(\infty, 2D)}(\mathbf{0}, \mathbf{0}; \varepsilon)$ is given in figure 2.

Appendix B. Topological features of a magnetic system in a finite volume

It has been well-known in condensed matter physics that the Bloch electron in a magnetic field yields a non-trivial topology [80]. The non-trivial topology of a magnetic system can be visually illustrated simply by using the twisted boundary condition given in equation (A3). Two edges of enlarged magnetic cubic box at $r_x = 0$ and $r_x = n_q L$ are glued together by a twist in the phase of wavefunction:

$$\psi_\varepsilon^{(L, \frac{\mathbf{P}_B}{2})}(n_q L, r_y) = e^{i \frac{\mathbf{P}_B}{2} \cdot \mathbf{n}_B L} e^{-i \varphi(r_y)} \psi_\varepsilon^{(L, \frac{\mathbf{P}_B}{2})}(0, r_y), \quad (\text{B1})$$

where

$$\varphi(r_y) = q B n_q L r_y = 2\pi n_p \frac{r_y}{L} \quad (\text{B2})$$

is the twisted phase of wavefunction along the circle of $r_y \in [0, L]$ that is a cross section of a torus with a fixed r_x . How much of twists in the phase is totally determined by n_p . Hence, the phase rotation of $\varphi(r_y)$ along the circle of r_y in fact form a geometry of n_p times twisted Möbius strip, see an example in figure 3, which demonstrates a non-trivial topology.

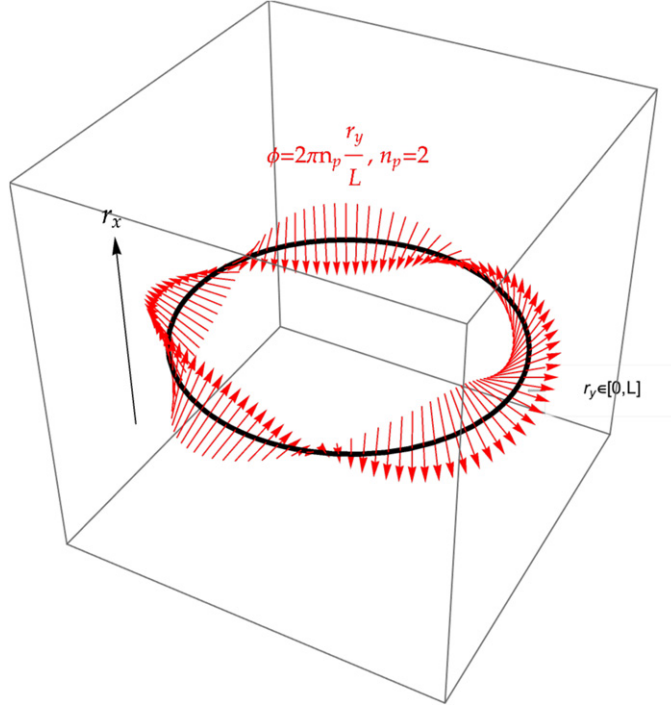


Figure 3. The plot of rotation of phase $\varphi(r_y)$ defined in equation (B2) along a cross section of a torus with a fixed r_x (black circle). The phase changes of $\varphi(r_y)$ on the circle of r_y is represented by the rotation of red arrows.

B.1. \mathbf{k} -space and Brillouin zone

Although in LQCD, the parameter \mathbf{P}_B is associated with the plane wave of CM motion of two-particle system, $e^{i\mathbf{P}_B \cdot \mathbf{R}}$, see reference [29]. Requirement of periodic boundary condition in CM motion yields the discrete value of \mathbf{P}_B 's in equation (A5), and discrete energy spectra as well. To further examine some non-trivial topological features and analytic properties of a magnetic system in finite volume, from now on, the discrete magnetic lattice vector $\frac{\mathbf{P}_B}{2}$ is replaced by a continuous wave vector \mathbf{k} that is analogous to the crystal momentum in condensed matter physics. In current section and also section 2, the wave vector \mathbf{k} are limited in real space. The continuous distribution of wave vector \mathbf{k} allows the introduction of Berry phase that is defined in a real \mathbf{k} -space [80, 89]. The Berry phase is a phase angle that describes the global phase evolution of the wavefunction of a system in a closed path in \mathbf{k} -space. Due to the fact that the same physical state is represented by a ray of wavefunctions that differ by a phase, such as $|\psi\rangle$ and $|\psi'\rangle = e^{i\phi}|\psi\rangle$, the set of phase factor $e^{i\phi}$ form a $U(1)$ group. Hence the ray of wavefunctions that are connected by a phase factor define a $U(1)$ fibre in a manifold of \mathbf{k} -space. Therefore, Berry phase is also recognized as a topological holonomy of the connection defined in a $U(1)$ fibre bundle in a parameter space [90], which is \mathbf{k} -space in our case. Berry phase is an important physical quantity that measures the topological feature of a system in a parameter space.

When \mathbf{k} is varied continuously, the discrete energy spectra are smeared into energy bands, also called bulk energy bands. These energy bands are separated by forbidden gaps between them due to the particle interactions. Each single allowed energy band hence becomes an isolated island in totally periodic systems. It has been known that the edge effects in a non-trivial

topological system may allow the gapless energy solutions [83, 84], which yields a continuous and smooth connection between two isolated energy bands. The topological edge solutions in a magnetic system will be discussed in section 2. In addition, when wave vector \mathbf{k} is further extended into a complex plane, given certain paths, the real energy solutions in the gap can also be found, which also connect two isolated energy bands smoothly. The discussion of analytic continuation of solutions in forbidden gaps will be presented in appendix C.

Using equation (A10), one can show easily that

$$G_B^{(L, \mathbf{k} + \mathbf{G}, 2D)}(\boldsymbol{\rho}, \boldsymbol{\rho}'; \varepsilon) = G_B^{(L, \mathbf{k})}(\boldsymbol{\rho}, \boldsymbol{\rho}'; \varepsilon), \quad (\text{B3})$$

where

$$\mathbf{G} = \frac{2\pi}{n_q L} \mathbf{e}_x + \frac{2\pi}{L} \mathbf{e}_y, \quad (\text{B4})$$

hence $\psi_\varepsilon^{(L, \mathbf{k} + \mathbf{G}, 2D)}(\boldsymbol{\rho})$ satisfies LS equation

$$\begin{aligned} & \psi_\varepsilon^{(L, \mathbf{k} + \mathbf{G}, 2D)}(\boldsymbol{\rho}) \\ &= \int_{L_B^2} d\boldsymbol{\rho}' G_B^{(L, \mathbf{k})}(\boldsymbol{\rho}, \boldsymbol{\rho}'; \varepsilon) V^{(L)}(\boldsymbol{\rho}') \psi_\varepsilon^{(L, \mathbf{k} + \mathbf{G}, 2D)}(\boldsymbol{\rho}'), \end{aligned} \quad (\text{B5})$$

so does $\psi_\varepsilon^{(L, \mathbf{k}, 2D)}(\boldsymbol{\rho})$. Therefore $\psi_\varepsilon^{(L, \mathbf{k} + \mathbf{G}, 2D)}(\boldsymbol{\rho})$ and $\psi_\varepsilon^{(L, \mathbf{k}, 2D)}(\boldsymbol{\rho})$ can only differ by a arbitrary phase factor, such as,

$$\psi_\varepsilon^{(L, \mathbf{k} + \mathbf{G}, 2D)}(\boldsymbol{\rho}) = \psi_\varepsilon^{(L, \mathbf{k}, 2D)}(\boldsymbol{\rho}), \quad (\text{B6})$$

and they both describe the same physical state. Therefore $\mathbf{k} + \mathbf{G}$ and \mathbf{k} are identified as the same point. The wave vector \mathbf{k} hence can be limited in first magnetic Brillouin zone,

$$k_x \in \left[0, \frac{2\pi}{n_q L}\right], \quad k_y \in \left[0, \frac{2\pi}{L}\right], \quad (\text{B7})$$

and the entire Brillouin zone form the geometry of a torus.

B.2. Berry phase and Berry vector potential

The non-trivial topology of magnetic system in finite volume results in a non-zero Berry phase. The Berry phase is defined crossing over the torus of entire Brillouin zone by

$$\begin{aligned} \gamma_\varepsilon &= \int_0^{\frac{2\pi}{L}} dk_y \left[A_{\varepsilon, y} \left(\frac{2\pi}{n_q L}, k_y \right) - A_{\varepsilon, y}(0, k_y) \right] \\ &\quad - \int_0^{\frac{2\pi}{n_q L}} dk_x \left[A_{\varepsilon, x} \left(k_x, \frac{2\pi}{L} \right) - A_{\varepsilon, x}(k_x, 0) \right], \end{aligned} \quad (\text{B8})$$

where Berry vector potential $\mathbf{A}(k_x, k_y)$ is given by

$$\mathbf{A}_\varepsilon(k_x, k_y) = \int_{L_B^2} d\boldsymbol{\rho} u_\varepsilon^{(\mathbf{k}, 2D)*}(\boldsymbol{\rho}) i \nabla_{\mathbf{k}} u_\varepsilon^{(\mathbf{k}, 2D)}(\boldsymbol{\rho}), \quad (\text{B9})$$

and $u_\varepsilon^{(\mathbf{k}, 2D)}(\boldsymbol{\rho})$ stands for the Bloch wavefunction and is related to $\psi_\varepsilon^{(L, \mathbf{k}, 2D)}(\boldsymbol{\rho})$ by

$$\psi_\varepsilon^{(L, \mathbf{k}, 2D)}(\boldsymbol{\rho}) = e^{i\mathbf{k} \cdot \boldsymbol{\rho}} u_\varepsilon^{(\mathbf{k}, 2D)}(\boldsymbol{\rho}). \quad (\text{B10})$$

The Berry phase over the torus of entire Brillouin zone is in fact a topological invariant quantity and quantized as 2π multiplied by an integer that is known as a Chern number [90].

In general, the Berry phase must be computed numerically by solving eigenvalue problems. In presence of particles interactions, the wavefunction must be given by linear superposition of

$$\psi_{\varepsilon}^{(L,\mathbf{k},2D)}(\boldsymbol{\rho}) = \sum_{n=0}^{\infty} \sum_{\alpha=0}^{n_p-1} c_{n,\alpha}^{(\mathbf{k})}(\varepsilon) \chi_{n,\alpha}^{(\mathbf{k})}(\boldsymbol{\rho}). \quad (\text{B11})$$

The coefficient $c_{n,\alpha}^{(\mathbf{k})}(\varepsilon)$ satisfies a matrix equation,

$$H^{(\mathbf{k})} c^{(\mathbf{k})}(\varepsilon) = \varepsilon c^{(\mathbf{k})}(\varepsilon), \quad (\text{B12})$$

where the matrix elements of effective Hamiltonian $H^{(\mathbf{k})}$ are given by

$$H_{n,\alpha;n',\alpha'}^{(\mathbf{k})} = \delta_{n,\alpha;n',\alpha'} \frac{qB}{\mu} \left(n + \frac{1}{2} \right) + V_{n,\alpha;n',\alpha'}^{(\mathbf{k})}, \quad (\text{B13})$$

and $V_{n,\alpha;n',\alpha'}^{(\mathbf{k})}$ is defined in equation (A31). The wave vector \mathbf{k} in equation (B12) is now treated as the parameter of dynamics of system, and ultimately, adiabatic evolution of \mathbf{k} crossing over magnetic Brillouin zone yields a Berry phase [80].

Since Berry phase is a topological invariance and also a robust quantity against particle interactions, non-trivial topological feature of a magnetic system in finite volume can be demonstrated by only using solutions of zero particle interactions. For a fixed n , there are n_p degenerate states,

$$u_{n,\alpha}^{(\mathbf{k})}(\boldsymbol{\rho}) = e^{-i\mathbf{k}\cdot\boldsymbol{\rho}} \chi_{n,\alpha}^{(\mathbf{k})}(\boldsymbol{\rho}). \quad (\text{B14})$$

The Berry phase for degenerate states $u_{n,\alpha}^{(\mathbf{k})}(\boldsymbol{\rho})$ with a fixed n is defined by the trace of Berry phase for each state [91],

$$\gamma_n = \sum_{\alpha=0}^{n_p-1} \gamma_{n,\alpha}, \quad (\text{B15})$$

where $\gamma_{n,\alpha}$ is defined in equation (B8) with Berry vector potential,

$$\mathbf{A}_{n,\alpha}(k_x, k_y) = \int_{L_B^2} d\rho u_{n,\alpha}^{(\mathbf{k})*}(\boldsymbol{\rho}) i \nabla_{\mathbf{k}} u_{n,\alpha}^{(\mathbf{k})}(\boldsymbol{\rho}). \quad (\text{B16})$$

Using relations of 1D harmonic oscillator eigen-solutions,

$$\begin{aligned} \sqrt{qBr_x} \phi_n(r_x) &= \sqrt{\frac{n+1}{2}} \phi_{n+1}(r_x) + \sqrt{\frac{n}{2}} \phi_{n-1}(r_x), \\ \partial_{\sqrt{qBr_x}} \phi_n(r_x) &= -\sqrt{\frac{n+1}{2}} \phi_{n+1}(r_x) + \sqrt{\frac{n}{2}} \phi_{n-1}(r_x), \end{aligned} \quad (\text{B17})$$

we find

$$\begin{aligned}
 i\partial_{k_x} u_{n,\alpha}^{(\mathbf{k})}(\boldsymbol{\rho}) &= \frac{1}{\sqrt{qB}} \left[\sqrt{\frac{n+1}{2}} u_{n+1,\alpha}^{(\mathbf{k})}(\boldsymbol{\rho}) + \sqrt{\frac{n}{2}} u_{n-1,\alpha}^{(\mathbf{k})}(\boldsymbol{\rho}) \right] \\
 &\quad - \left(\frac{\frac{2\pi\alpha}{L} + k_y}{qB} \right) u_{n,\alpha}^{(\mathbf{k})}(\boldsymbol{\rho}), i\partial_{k_y} u_{n,\alpha}^{(\mathbf{k})}(\boldsymbol{\rho}) \\
 &= -\frac{i}{\sqrt{qB}} \left[\sqrt{\frac{n+1}{2}} u_{n+1,\alpha}^{(\mathbf{k})}(\boldsymbol{\rho}) - \sqrt{\frac{n}{2}} u_{n-1,\alpha}^{(\mathbf{k})}(\boldsymbol{\rho}) \right].
 \end{aligned} \tag{B18}$$

Also using orthogonality relation given in equation (A25), we thus obtain

$$A_{n,\alpha,x}(k_x, k_y) = -\left(\frac{\frac{2\pi\alpha}{L} + k_y}{qB} \right), \tag{B19}$$

$$A_{n,\alpha,y}(k_x, k_y) = 0.$$

Hence, the Berry phases are given by

$$\gamma_{n,\alpha} = \frac{2\pi}{n_p}, \quad \frac{\gamma_n}{2\pi} = 1. \tag{B20}$$

B.3. Topological properties of $\chi_{n,\alpha}^{(\mathbf{k})}$ functions

The Berry phase of a magnetic system in finite volume can also be understood by simply examining the topological properties of $\chi_{n,\alpha}^{(\mathbf{k})}$ functions.

Using equation (A20), one can show that how the center of $\chi_{n,\alpha}^{(\mathbf{k})}$ function is pushed along x -direction when the wave vector \mathbf{k} is forced to change in y -direction,

$$\chi_{n,\alpha}^{(\mathbf{k}+\Delta k_y \mathbf{e}_y)}(\boldsymbol{\rho}) = e^{i\Delta k_y r_y} \chi_{n,\alpha}^{(\mathbf{k})} \left(\boldsymbol{\rho} + \frac{\Delta k_y}{qB} \mathbf{e}_x \right). \tag{B21}$$

Thus equation (B21) yields

$$\chi_{n,\alpha}^{(\mathbf{k}+\frac{2\pi}{L} \frac{n_p}{n_q} \mathbf{e}_y)}(\boldsymbol{\rho}) = e^{iqBLr_y} \chi_{n,\alpha}^{(\mathbf{k})}(\boldsymbol{\rho} + L\mathbf{e}_x), \tag{B22}$$

that is to say, to move the center of $\chi_{n,\alpha}^{(\mathbf{k})}$ by length- L in x -direction, it requires the change of wave vector \mathbf{k} by $\frac{2\pi}{L} \frac{n_p}{n_q}$ in y -direction.

When \mathbf{k} is forced to move across entire Brillouin zone in y -direction,

$$\chi_{n,\alpha}^{(\mathbf{k}+\frac{2\pi}{L} \mathbf{e}_y)}(\boldsymbol{\rho}) = e^{i\frac{2\pi}{L} r_y} \chi_{n,\alpha}^{(\mathbf{k})} \left(\boldsymbol{\rho} + \frac{n_q L}{n_p} \mathbf{e}_x \right) = \chi_{n,\alpha+1}^{(\mathbf{k})}(\boldsymbol{\rho}), \tag{B23}$$

the center of $\chi_{n,\alpha}^{(\mathbf{k})}$ function is only moved by $\frac{n_q L}{n_p}$ in x -direction, which is then smoothly connected to the $\chi_{n,\alpha+1}^{(\mathbf{k})}$ function. Hence, an array of states

$$\chi_n^{(\mathbf{k})} = \left[\chi_{n,0}^{(\mathbf{k})}, \chi_{n,1}^{(\mathbf{k})}, \dots, \chi_{n,n_p-1}^{(\mathbf{k})} \right], \tag{B24}$$

behaves as a n_p components spinor. $\Delta k_y = \frac{2\pi}{L}$ plays the role of raising operator which change each individual component of spinor $\chi_n^{(\mathbf{k})}$ by one unit,

$$\chi_n^{\left(\mathbf{k} + \frac{2\pi}{L}\mathbf{e}_y\right)} = \left[\chi_{n,1}^{(\mathbf{k})}, \chi_{n,2}^{(\mathbf{k})}, \dots, \chi_{n,n_p}^{(\mathbf{k})} \right]. \quad (\text{B25})$$

Operating raising operator n_p times, with the help of periodic boundary condition, we can also show that

$$\begin{aligned} \chi_{n,\alpha}^{\left(\mathbf{k} + \frac{2\pi}{L}n_p\mathbf{e}_y\right)}(\boldsymbol{\rho}) &= e^{i\frac{2\pi}{L}n_p r_y} \chi_{n,\alpha}^{(\mathbf{k})}(\boldsymbol{\rho} + n_q L \mathbf{e}_x) = \chi_{n,\alpha+n_p}^{(\mathbf{k})}(\boldsymbol{\rho}) \\ &= e^{ik_x n_q L} \chi_{n,\alpha}^{(\mathbf{k})}(\boldsymbol{\rho}). \end{aligned} \quad (\text{B26})$$

Therefore,

$$\chi_n^{\left(\mathbf{k} + \frac{2\pi}{L}\mathbf{e}_y\right)} = \left[\chi_{n,1}^{(\mathbf{k})}, \chi_{n,2}^{(\mathbf{k})}, \dots, e^{ik_x n_q L} \chi_{n,0}^{(\mathbf{k})} \right], \quad (\text{B27})$$

changing \mathbf{k} by $\frac{2\pi}{L}\mathbf{e}_y$ leads to the circulation of all components only once, and only the component sitting at right edge of spinor gains a phase factor, $e^{ik_x n_q L}$. On the other hand, changing \mathbf{k} by $\frac{2\pi}{L}n_p\mathbf{e}_y$ however yields that the center of each component of spinor $\chi_n^{(\mathbf{k})}$ is forced to wind around entire magnetic unit cell in x -direction. Meanwhile, all components of the spinor circulate n_p times and come back to the starting point, so each one has a chance to gain a phase factor $e^{ik_x n_q L}$ when it reaches the right edge of spinor,

$$\chi_n^{\left(\mathbf{k} + \frac{2\pi}{L}n_p\mathbf{e}_y\right)} = e^{ik_x n_q L} \chi_n^{(\mathbf{k})}. \quad (\text{B28})$$

In addition, when the wave vector \mathbf{k} is forced to move across magnetic Brillouin zone in x -direction, the each component of spinor $\chi_n^{(\mathbf{k})}$ remains at the same location in a spinor,

$$\chi_{n,\alpha}^{\left(\mathbf{k} + \frac{2\pi}{n_q L}\mathbf{e}_x\right)}(\boldsymbol{\rho}) = \chi_{n,\alpha}^{(\mathbf{k})}(\boldsymbol{\rho}), \quad (\text{B29})$$

and

$$\chi_n^{\left(\mathbf{k} + \frac{2\pi}{n_q L}\mathbf{e}_x\right)} = \chi_n^{(\mathbf{k})}. \quad (\text{B30})$$

Now, the non-trivial Berry phase may also be understood simply by using the properties given in equations (B27) and (B30). Assuming that we start at one corner of Brillouin zone: $\mathbf{k} = (0, 0)$ with initial spinor of

$$\chi_n^{(i)} = \left[\chi_{n,0}^{(0,0)}, \chi_{n,1}^{(0,0)}, \dots, \chi_{n,n_p-1}^{(0,0)} \right], \quad (\text{B31})$$

where i is used to label initial state of spinor, then we start moving around the boundary of magnetic Brillouin zone counter-clock wise,

$$\mathbf{k} : (0, 0) \xrightarrow{(1)} \left(\frac{2\pi}{n_q L}, 0 \right) \xrightarrow{(2)} \left(\frac{2\pi}{n_q L}, \frac{2\pi}{L} \right) \xrightarrow{(3)} \left(0, \frac{2\pi}{L} \right) \xrightarrow{(4)} (0, 0). \quad (\text{B32})$$

At step (1), moving from $\mathbf{k} = (0, 0)$ to $\left(\frac{2\pi}{n_q L}, 0\right)$ by an increase of $\Delta k_x = \frac{2\pi}{n_q L}$, there is no phase change,

$$\chi_n^{\left(\frac{2\pi}{n_q L}, 0\right)} = \chi_n^{(i)}. \quad (\text{B33})$$

At step (2), moving from $(\frac{2\pi}{n_q L}, 0)$ to $(\frac{2\pi}{n_q L}, \frac{2\pi}{L})$ by an increase of $\Delta k_y = \frac{2\pi}{L}$, we find

$$\chi_n^{(\frac{2\pi}{n_q L}, \frac{2\pi}{L})} = \left[\chi_{n,1}^{(0,0)}, \chi_{n,2}^{(0,0)}, \dots, e^{i\frac{2\pi}{n_q L} n_q L} \chi_{n,0}^{(0,0)} \right]. \tag{B34}$$

At step (3), moving from $(\frac{2\pi}{n_q L}, \frac{2\pi}{L})$ to $(0, \frac{2\pi}{L})$ by a decrease of $\Delta k_x = -\frac{2\pi}{n_q L}$, there is again no phase change, so that

$$\chi_n^{(0, \frac{2\pi}{L})} = \chi_n^{(\frac{2\pi}{n_q L}, \frac{2\pi}{L})}. \tag{B35}$$

At last step (4), moving from $(0, \frac{2\pi}{L})$ back to $(0, 0)$ by a decrease of $\Delta k_y = -\frac{2\pi}{L}$, although there is no phase change at last step, all components of spinor are moved down by one unit, so that the final state of spinor is given by

$$\chi_n^{(f)} = \left[\chi_{n,0}^{(0,0)}, \chi_{n,1}^{(0,0)}, \dots, e^{i\frac{2\pi}{n_q L} n_q L} \chi_{n,n_p-1}^{(0,0)} \right]. \tag{B36}$$

Therefore, the phase difference between initial and final states is given by

$$-\sum_{\alpha=0}^{n_p-1} \text{Im} \ln \langle \chi_{n,\alpha}^{(f)} | \chi_{n,\alpha}^{(i)} \rangle = \frac{2\pi}{n_q L} n_q L = 2\pi, \tag{B37}$$

which can be identified as Berry phase γ_n .

The Berry phase is the quantity that describes the accumulation of a global phase of a system's wavefunction as the \mathbf{k} is carried around the torus of Brillouin zone, non-zero value of Berry phase hence represents a topological obstruction to the determination of the phase of wavefunction [81] over entire Brillouin zone. For a magnetic system, the magnetic field create a vortex-like singularities in wavefunctions that attribute to a non-trivial topology of a magnetic system. The vortex-like singularities can be illustrated analytically by $\chi_{0,\alpha}^{(\mathbf{k})}(\rho)$. Using equation (A20) and $H_0(x) = 1$, we find

$$\begin{aligned} \Theta_{\alpha}^{(\mathbf{k})}(\rho) &= e^{-i(k_y + \frac{2\pi\alpha}{L})r_y} \chi_{0,\alpha}^{(\mathbf{k})}(\rho) \\ &= \frac{1}{\sqrt{L}} \left(\frac{qB}{\pi} \right)^{\frac{1}{4}} e^{-\frac{qB}{2} \left(r_x + \frac{k_y + \frac{2\pi\alpha}{L}}{qB} \right)^2} \\ &\quad \times \vartheta_3 \left(\frac{\pi n_p}{L} \left[\left(r_y - \frac{k_x}{qB} \right) + i \left(r_x + \frac{k_y + \frac{2\pi\alpha}{L}}{qB} \right) \right], e^{-\pi n_p n_q} \right), \end{aligned} \tag{B38}$$

where $\vartheta_3(z, q)$ is Jacobi's theta function [78], and defined by

$$\vartheta_3(z, q) = 1 + 2 \sum_{n=1}^{\infty} q^{n^2} \cos(2nz). \tag{B39}$$

The zeros of

$$\vartheta_3(z, q = e^{i\pi\tau})$$

are determined by linear equation,

$$z = \left(n_1 + \frac{1}{2} \right) \pi + \left(n_2 + \frac{1}{2} \right) \tau \pi, \quad (n_1, n_2) \in \mathbb{Z}, \tag{B40}$$

hence, the locations of zeros of $\chi_{0,\alpha}^{(\mathbf{k})}(\boldsymbol{\rho})$ are given by

$$\begin{aligned} r_y - \frac{k_x}{qB} &= \left(n_1 + \frac{1}{2}\right) \frac{L}{n_p}, \quad n_1 \in \mathbb{Z}, \\ r_x + \frac{k_y}{qB} + \frac{2\pi\alpha}{qB} &= \left(n_2 + \frac{1}{2}\right) n_q L, \quad n_2 \in \mathbb{Z}. \end{aligned} \quad (\text{B41})$$

The zeros of $\chi_{0,\alpha}^{(\mathbf{k})}(\boldsymbol{\rho})$ present vortex-like singularities, which ultimately create discontinuity of phase of $\chi_{0,\alpha}^{(\mathbf{k})}(\boldsymbol{\rho})$ in both $\boldsymbol{\rho}$ - and \mathbf{k} -space. The $\vartheta_3(z, q)$ is a real function when z values are real and $|q| < 1$, therefore, for a fixed \mathbf{k} ,

$$\text{Im}\left[\Theta_\alpha^{(\mathbf{k})}(\boldsymbol{\rho})\right]_{\boldsymbol{\rho}=\left(-\frac{k_y + \frac{2\pi\alpha}{qB}}{qB}, r_y\right)} = 0, \quad (\text{B42})$$

thus the phase of $\chi_{0,\alpha}^{(\mathbf{k})}(\boldsymbol{\rho})$ is not well-defined along the line of $\left(-\frac{k_y + \frac{2\pi\alpha}{qB}}{qB}, r_y\right)$ in $\boldsymbol{\rho}$ -space. On the other hand, for a fixed $\boldsymbol{\rho}$,

$$\text{Im}\left[\Theta_\alpha^{(\mathbf{k})}(\boldsymbol{\rho})\right]_{\mathbf{k}=\left(k_x, -\frac{2\pi\alpha}{L} - qBr_y\right)} = 0, \quad (\text{B43})$$

so in \mathbf{k} -space, the phase is also not well-defined along the line of $\left(k_x, -\frac{2\pi\alpha}{L} - qBr_y\right)$. These two lines cut through both entire $\boldsymbol{\rho}$ - and \mathbf{k} -space. Because of asymmetry of $\Theta_\alpha^{(\mathbf{k})}(\boldsymbol{\rho})$ along these two lines, it creates the mismatch of the phase of $\chi_{0,\alpha}^{(\mathbf{k})}(\boldsymbol{\rho})$ on half portion of the line, which starts at the location of zeros of $\chi_{0,\alpha}^{(\mathbf{k})}(\boldsymbol{\rho})$, see figure 4 as an example of phase mismatch. These vortex-like singularities in wavefunction is similar to the branch point singularities in complex analysis, the vortex creates a cut in both $\boldsymbol{\rho}$ - and \mathbf{k} -space, and phase of wavefunction along the cut has a discontinuity. Hence, when particle is forced to wind around the vortex, the phase of wavefunction has a jump which account how many times the winding number of motion around the vortex.

The phase discontinuity of $\chi_{n,\alpha}^{(\mathbf{k})}(\boldsymbol{\rho})$ ultimately creates non-trivial topology of the Berry vector potential given in equation (B19). The vortex-like singularities not only create discontinuity of phase in wavefunction, but also leads to the mismatch of Berry vector potential on the torus of entire magnetic Brillouin zone. Since the torus has no boundary, uniquely and smoothly defined Berry vector potential on the torus results in the trivial topology and vanishing Berry phase. For $\chi_{n,\alpha}^{(\mathbf{k})}(\boldsymbol{\rho})$ wavefunction, according to equation (B19), it is clearly that the Berry vector potential on the lower edge of torus along the line $\mathbf{k} = (k_x, 0)$ is

$$\mathbf{A}_{n,\alpha}(k_x, 0) = -\alpha \frac{n_q L}{n_p} \mathbf{e}_x. \quad (\text{B44})$$

On the upper edge of torus along the line of $\mathbf{k} = \left(k_x, \frac{2\pi}{L}\right)$, the Berry vector potential is

$$\mathbf{A}_{n,\alpha}\left(k_x, \frac{2\pi}{L}\right) = -(\alpha + 1) \frac{n_q L}{n_p} \mathbf{e}_x. \quad (\text{B45})$$

The upper and lower edges of a torus is considered as the same points, hence, magnetic field ultimately cause a mismatch of Berry vector potential on the torus, see figure 5 as an example. The discontinuity of Berry vector potential is given by

$$\mathbf{A}_{n,\alpha}\left(k_x, \frac{2\pi}{L}\right) - \mathbf{A}_{n,\alpha}(k_x, 0) = -\frac{n_q L}{n_p} \mathbf{e}_x, \quad (\text{B46})$$

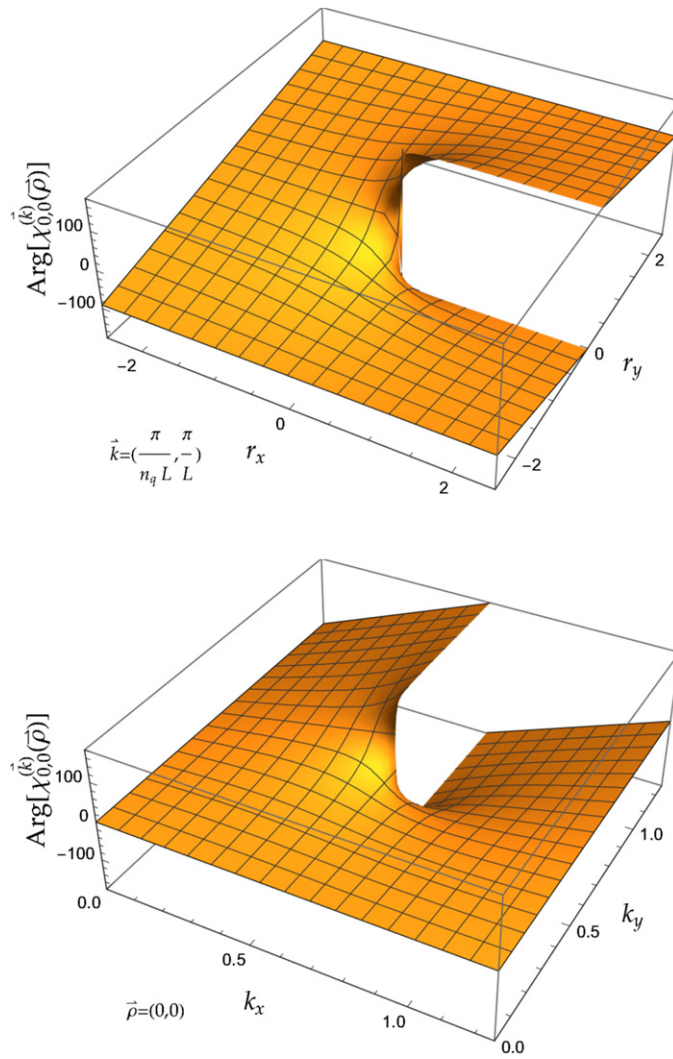


Figure 4. The phase plot of $\chi_{0,0}^{(k)}(\rho)$ with fixed $\mathbf{k} = (\frac{\pi}{L}, \frac{\pi}{L})$ in ρ -space (upper panel) vs phase plot of $\chi_{0,0}^{(k)}(\rho)$ with fixed $\rho = (0, 0)$ in \mathbf{k} -space (lower panel). The parameters are chosen as: $L = 5$ and $n_p = n_q = 1$.

which ultimately leads to a non-zero Berry phase. The discontinuity of Berry vector potential on a closed path in \mathbf{k} -space is known as a holonomy [90]. When wave vector \mathbf{k} is forced to move along a closed path, the Berry vector potential then generates a horizontal lift of the wavefunction along the $U(1)$ fibre of each state, hence, in adiabatic limit, the states along the path in \mathbf{k} -space are all connected by

$$u_{n,\alpha}^{(\mathbf{k}(t))}(\rho) \sim e^{-i \int_{\mathbf{k}(0)}^{\mathbf{k}(t)} \mathbf{A}_{n,\alpha}(\mathbf{k}) \cdot d\mathbf{k}} u_{n,\alpha}^{(\mathbf{k}(0))}(\rho). \tag{B47}$$

Each state on the path has the memory of previous states along the path. The holonomy of a system detects a topological or geometric nature of the underlying structure of the physical system.

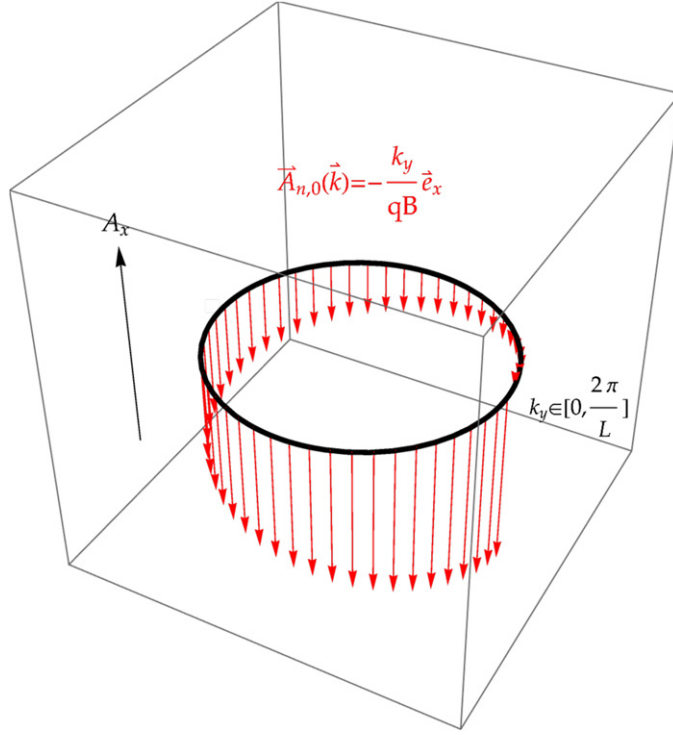


Figure 5. The plot of Berry vector potential $\mathbf{A}_{n,0}(k_x, k_y)$ on a cross section of torus of Brillouin zone with a fixed k_x . The parameters are chosen as: $L = 5$ and $n_p = n_q = 1$.

The twisting of $U(1)$ fibre bundle results in the non-trivial value of holonomy. The twisting of $U(1)$ fibre bundle in \mathbf{k} -space can be understood by the relation given in equation (B26), which yields

$$u_{n,\alpha}^{(k_x, \frac{2\pi}{L}n_p)}(\boldsymbol{\rho}) = e^{-i\frac{2\pi}{L}n_p r_y} e^{i\tilde{\varphi}(k_x)} u_{n,\alpha}^{(k_x,0)}(\boldsymbol{\rho}), \tag{B48}$$

where

$$\tilde{\varphi}(k_x) = k_x n_q L. \tag{B49}$$

Equation (B48) may be interpreted as twisted boundary condition in enlarged Brillouin zone:

$$k_x \in \left[0, \frac{2\pi}{n_q L}\right], \quad k_y \in \left[0, \frac{2\pi}{L}n_p\right]. \tag{B50}$$

Hence, similar to twisted boundary condition in equation (B1) in $\boldsymbol{\rho}$ -space, when two edges at $k_y = 0$ and $k_y = \frac{2\pi}{L}n_p$ of enlarged Brillouin zone are glued together, $\tilde{\varphi}(k_x)$ describes the twisted phase of wavefunction along the circle of $k_x \in [0, \frac{2\pi}{n_q L}]$.

We also remark that noticing that equation (B18) may be rearranged to

$$\sum_{n',\alpha'} [\delta_{n,\alpha;n',\alpha'} \nabla_{\mathbf{k}} + i\mathbf{A}_{n,\alpha;n',\alpha'}(\mathbf{k})] u_{n',\alpha'}^{(\mathbf{k})}(\boldsymbol{\rho}) = 0, \tag{B51}$$

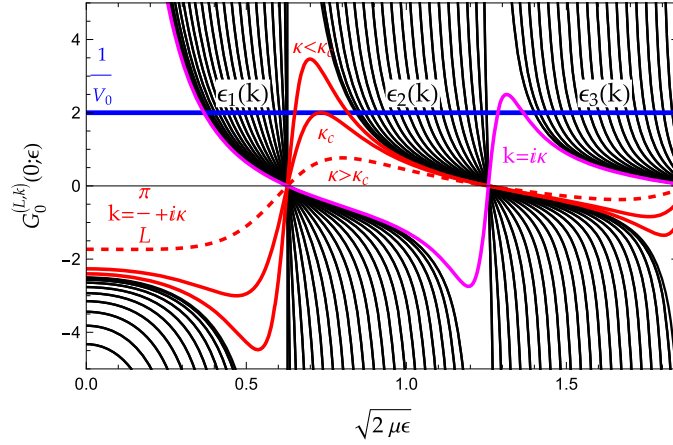


Figure 6. Plot of $G_0^{(L,k)}(0; \epsilon)$ defined in equation (C2) vs $\frac{1}{V_0}$ (blue solid line): the area of allowed energy bands are filled by black curves (real $k \in [0, \frac{2\pi}{L}]$ values), the energy bands are separated by gaps; the red and purple curves that show up in gaps are generated with complex wave vectors $k = \frac{\pi}{L} + i\kappa$ and $k = i\kappa$ respectively. A pair of energy solutions in the gap can be found for $\kappa < \kappa_c$. The parameters are: $V_0 = 0.5$, $\mu = 1$ and $L = 5$.

where the matrix elements of Berry vector potential matrix are given by

$$\begin{aligned}
 \mathbf{A}_{n,\alpha;n',\alpha'}(\mathbf{k}) &= \int_{L_B^2} d\rho u_{n,\alpha}^{(\mathbf{k})*}(\rho) i \nabla_{\mathbf{k}} u_{n',\alpha'}^{(\mathbf{k})}(\rho) \\
 &= \frac{1}{\sqrt{qB}} \sqrt{\frac{n+1}{2}} \delta_{n+1,n'} \delta_{\alpha,\alpha'} (\mathbf{e}_x - i\mathbf{e}_y) \\
 &\quad + \frac{1}{\sqrt{qB}} \sqrt{\frac{n}{2}} \delta_{n-1,n'} \delta_{\alpha,\alpha'} (\mathbf{e}_x + i\mathbf{e}_y) \\
 &\quad - \delta_{n,n'} \delta_{\alpha,\alpha'} \left(\frac{2\pi\alpha}{L} + k_y \right) \mathbf{e}_x.
 \end{aligned} \tag{B52}$$

Non-vanishing off-diagonal terms in Berry vector potential matrix suggest that a magnetic system may experience non-adiabatic transition between different eigen-states. For an example, assuming an non-interacting magnetic system, the general Bloch wavefunction is given by the linear superposition of eigen-states of non-interacting magnetic system,

$$u^{(\mathbf{k}(t))}(\rho) = \sum_{n,\alpha} c_{n,\alpha}(t) u_{n,\alpha}^{(\mathbf{k}(t))}(\rho), \tag{B53}$$

where t is used to parameterize the evolution of wave vector \mathbf{k} . Also assuming $u^{(\mathbf{k}(t))}(\rho)$ satisfies Schrödinger equation

$$i \partial_t u^{(\mathbf{k}(t))}(\rho) = \hat{H}_{\text{eff}}(\mathbf{k}(t)) u^{(\mathbf{k}(t))}(\rho), \tag{B54}$$

where $u_{n,\alpha}^{(\mathbf{k}(t))}(\boldsymbol{\rho})$ are eigen-solutions of $\hat{H}_{\text{eff}}(\mathbf{k}(t)) = e^{-i\mathbf{k}(t)\cdot\boldsymbol{\rho}}\hat{H}_{\rho}e^{i\mathbf{k}(t)\cdot\boldsymbol{\rho}}$,

$$\hat{H}_{\text{eff}}(\mathbf{k}(t))u_{n,\alpha}^{(\mathbf{k}(t))}(\boldsymbol{\rho}) = \frac{qB}{\mu} \left(n + \frac{1}{2} \right) u_{n,\alpha}^{(\mathbf{k}(t))}(\boldsymbol{\rho}), \quad (\text{B55})$$

thus, we find that the coefficient $c_{n,\alpha}(t)$ must satisfy equation,

$$i \frac{dc_{n,\alpha}(t)}{dt} = \frac{qB}{\mu} \left(n + \frac{1}{2} \right) c_{n,\alpha}(t) - \frac{d\mathbf{k}(t)}{dt} \cdot \sum_{n',\alpha'} \mathbf{A}_{n,\alpha;n',\alpha'}(\mathbf{k}) c_{n',\alpha'}(t). \quad (\text{B56})$$

Therefore, the diagonal term in Berry vector potential matrix yields the Berry phase in equation (B20) in the limit of adiabatic process, the off-diagonal terms may describes the transition among different eigen-states when \mathbf{k} is forced to increase or decrease.

Appendix C. Analytic properties of finite volume solutions

The periodicity of lattice structure and particles interaction create the band structures, the energy spectrum split into isolated bands separated by gaps in between. Hence, when wave vector \mathbf{k} is changed continuously, the energy of particle must experience a discontinuity when particle jumps from one band to another. It has been shown [92, 93] that when wave vector is taken complex at the edge of Brillouin zone, the real energy solutions in the gap are possible, hence the transition from one band to another can be made smoothly in complex \mathbf{k} plane. The complex wave vector at the edge of Brillouin zone may be interpreted as edge solutions with a penetrable wall on the edge or surface of material. In presence of a magnetic field, the real energy solutions can also be found for complex wave vector, however, the situation is more complicated, the energy solutions not only appear in the gap but also penetrate into bulk energy bands because of non-trivial topology.

In this section, we first give a brief summary of complex wave vector with a simple 1D example. With a contact interaction, the quantization condition in 1D is given by

$$\frac{1}{V_0} = G_0^{(L,k)}(0; \varepsilon), \quad (\text{C1})$$

where 1D finite volume Green's function is given by

$$\begin{aligned} \frac{1}{2\mu} G_0^{(L,k)}(0; \varepsilon) &= - \sum_{n \in \mathbb{Z}} \frac{i e^{i\sqrt{2\mu\varepsilon}|nL|}}{\sqrt{2\mu\varepsilon}} e^{-iknL} \\ &= - \frac{2\mu}{2\sqrt{2\mu\varepsilon}} \frac{\sin \sqrt{2\mu\varepsilon}L}{\cos \sqrt{2\mu\varepsilon}L - \cos kL}. \end{aligned} \quad (\text{C2})$$

The finite volume Green's function $G_0^{(L,k)}$ remains real as for the real value of k , which yields the real dispersion relation of

$$\varepsilon = \varepsilon(k) = \varepsilon(-k) = \varepsilon \left(k + \frac{2\pi}{L} \right). \quad (\text{C3})$$

The band structures is explicitly produced by the bound of $|\cos kL| \leq 1$. Using equation (C2), one can show that for $k = \frac{\pi d}{L} + i\kappa$, $d \in \mathbb{Z}$, Green's function is still a real function,

$$G_0^{\left(L, \frac{\pi d}{L} + i\kappa\right)}(0; \varepsilon) = - \frac{2\mu}{2\sqrt{2\mu\varepsilon}} \frac{\sin \sqrt{2\mu\varepsilon}L}{\cos \sqrt{2\mu\varepsilon}L - (-1)^d \cosh \kappa L}. \quad (\text{C4})$$

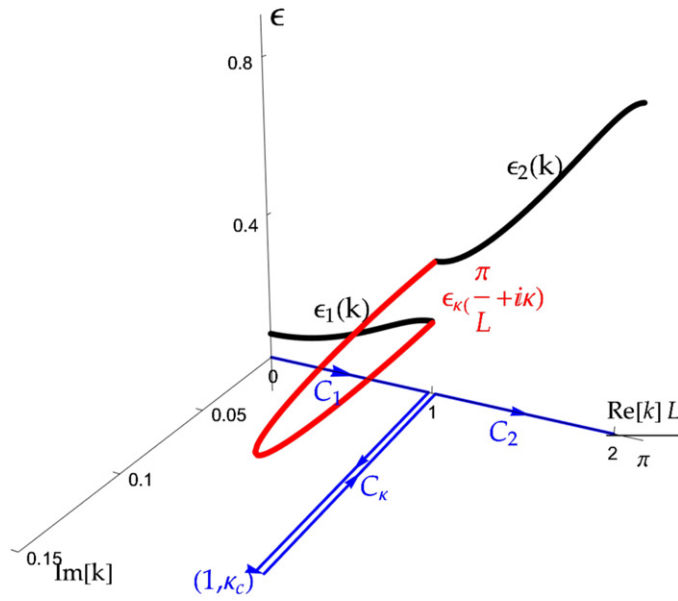


Figure 7. The motion of $\varepsilon(k)$ as the wave vector k moves continuously in complex plane follow the path: $C_1 \rightarrow C_\kappa \rightarrow C_2$. C_1 and C_2 are on real axis in k plane between $[0, \frac{\pi}{L}]$ and $[\frac{\pi}{L}, \frac{2\pi}{L}]$ respectively. C_κ is on complex plane with $k = \frac{\pi}{L} + i\kappa$, $\kappa : 0 \rightarrow \kappa_c \rightarrow 0$. The energy solutions thus moves continuously from $\varepsilon_1(k)$ into $\varepsilon_\kappa(\frac{\pi}{L} + i\kappa)$ in the gap, and then connected into $\varepsilon_2(k)$.

Hence, we can see clearly because of

$$\cosh \kappa L \geq 1,$$

the energy solutions of complex wave function, $k = \frac{\pi d}{L} + i\kappa$, only show up in the gaps between bands, see figure 6. In the gaps, for a fixed V_0 , a pair of energy solutions can be found for finite value of κ . The gap between two solutions shrinks when κ is increased, until κ reach its critical point κ_c , the gap close up, two solutions becomes degenerate. Beyond κ_c , no solutions can be found, see figure 6 as an example. Therefore, the complex wave vector can be used as a parameter to navigate across bulk energy bands smoothly. Using figure 7 as an example, two allowed energy bands $\varepsilon_1(k)$ and $\varepsilon_2(k)$ are separated by a gap for real values of k 's. Imaging wave vector k start at $k = 0$, and is forced to move following the path of $C_1 \rightarrow C_\kappa \rightarrow C_2$ in figure 7, where both C_1 and C_2 are defined on real axis for $k \in [0, \frac{\pi}{L}]$ and $k \in [\frac{\pi}{L}, \frac{2\pi}{L}]$ respectively. The contour C_κ is defined in complex k plane with fixed $\text{Re}[k] = \frac{\pi}{L}$ value, and the imaginary part of $\text{Im}[k] = \kappa$ is circling around κ_c , $\kappa : 0 \rightarrow \kappa_c \rightarrow 0$. While k is on C_1 , the energy solution stays in energy band $\varepsilon_1(k)$ following the motion of k , moving from lower edge $\varepsilon_1(0)$ up to upper edge $\varepsilon_1(\frac{\pi}{L})$. While k is extended into complex plane on C_κ , the energy solution then protrude into the gap between two allowed bands, and continue climbing up to the lower edge of energy band $\varepsilon_2(k)$ at $\varepsilon_2(\frac{\pi}{L})$. Then, it merged into second band $\varepsilon_2(k)$ if k is increased further on C_2 . Similarly, $\varepsilon_2(k)$ and $\varepsilon_3(k)$ are smoothly connected by taking wave vector into complex plane at the edge of Brillouin zone: $k = \frac{2\pi}{L} + i\kappa$ which is equivalent to $k = i\kappa$, see figure 6. We can also see from figure 6 that the curves of $G_0^{(L, \frac{\pi d}{L} + i\kappa)}(0; \varepsilon)$ with different d values occupy completely different territories, hence there are no degenerate energy solutions for different d values.

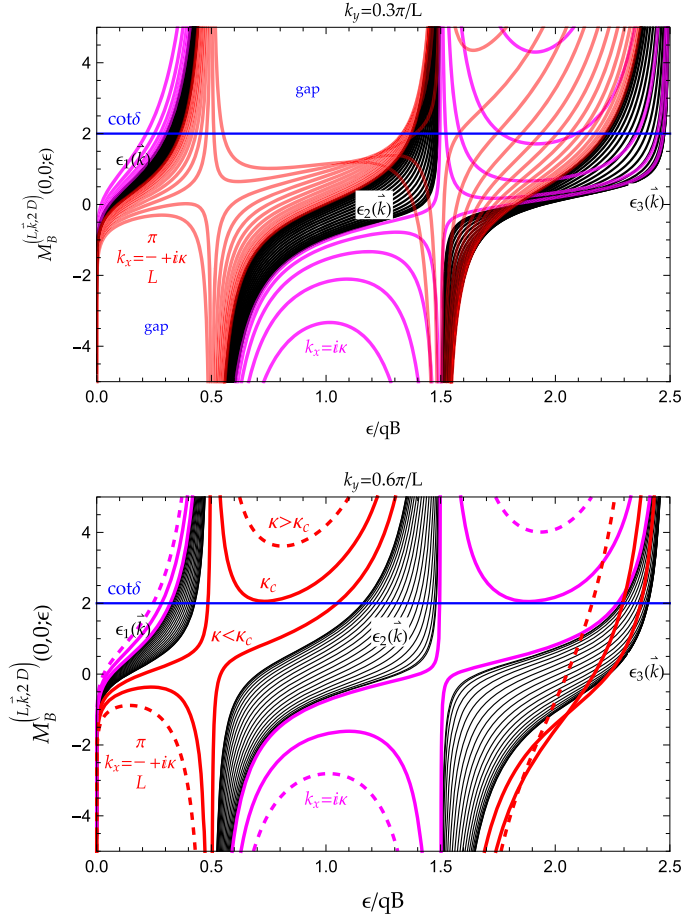


Figure 8. Energy band structure (filled with black curves) is the result of periodicity in both x - and y -direction, red ($d = 1$) and purple ($d = 0$) curves are generated by taking k_x into complex plane: $k_x = \frac{\pi d}{L} + i\kappa$. k_y 's are fixed at $k_y = 0.3\frac{\pi}{L}$ and $k_y = 0.6\frac{\pi}{L}$ in upper and lower panels respectively. The parameters are chosen as: $L = 5$, and $n_q = n_p = 1$. Blue line represents a constant $\cot \delta_0(\varepsilon)$ that is used only to help to visualize the energy solutions.

In presence of magnetic field, with a complex wave vector

$$\mathbf{k} = \left(\frac{\pi d}{n_q L} + i\kappa \right) \mathbf{e}_x + k_y \mathbf{e}_y, \quad d \in \mathbb{Z}, \quad (\text{C5})$$

similarly, the real energy solutions are also available, however situation becomes much more intriguing. Unfortunately, for a magnetic system, analytic properties cannot be shown easily in a straightforward way, all the discussions heavily rely on numerics. Let us consider the case of $n_q = 1$ as a simple example, which corresponds to a single contact interaction placed at origin, thus the magnetic zeta function is given by

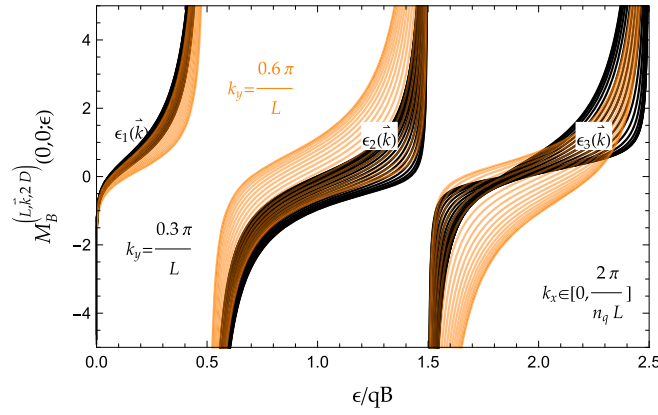


Figure 9. Overlapping energy bands of different k_y values: $k_y = 0.3\frac{\pi}{L}$ (black) vs $k_y = 0.6\frac{\pi}{L}$ (orange).

$$\begin{aligned}
 & \mathcal{M}_B^{(L, (\frac{\pi d}{n_q L} + i\kappa) \mathbf{e}_x + k_y \mathbf{e}_y, 2D)}(\mathbf{0}, \mathbf{0}; \epsilon) \\
 &= \mathcal{M}_B^{(\infty, 2D)}(\mathbf{0}, \mathbf{0}; \epsilon) \\
 &+ \frac{1}{\pi} \sum_{\mathbf{n}_B \neq \mathbf{0}} (-1)^{dn_x} (-1)^{n_p n_x n_y} e^{\kappa n_x n_q L} e^{-ik_y n_y L} \\
 &\times e^{-\frac{qB}{4} |\mathbf{n}_B L|^2} \Gamma\left(\frac{1}{2} - \frac{\mu\epsilon}{qB}\right) U\left(\frac{1}{2} - \frac{\mu\epsilon}{qB}, 1, \frac{qB}{2} |\mathbf{n}_B L|^2\right), \quad (C6)
 \end{aligned}$$

which is indeed a real function. Compared with previously discussed 1D topologically trivial example, there are some new features in a magnetic system. First of all, as we can see in figure 8, for small k_y , the gap area between allowed energy bands cannot be completely filled by taking k_x into complex plane, see gap between ϵ_1 and ϵ_2 bands in upper panel in figure 8. Hence, for certain range of k_y , although complex wave vector k_x may narrow the gap, the gap remains. Therefore, using complex k_x alone to navigate through gaps are not possible for certain range of k_y , however, due to overlapping energy bands of different k_y , see figure 9, it may be still possible by using both complex k_x and real k_y to navigate through different energy bands smoothly by avoiding gap area. Secondly, with complex wave vector $k_x = \frac{\pi d}{n_q L} + i\kappa$, curves not only show up in the gap areas, some curves punch through the allowed bulk bands, and invade into the gap areas with different d value, see figure 8. In addition, the curves with complex wave vectors in gap make up a vortex shape, all the curves are pushed away from a vortex centered at location of Landau level energy: $\epsilon_n = \frac{qB}{\mu}(n + \frac{1}{2})$, see example in figure 8. These irregular behaviors of magnetic zeta function with a complex wave vector may have a topological origin.

ORCID iDs

Peng Guo  <https://orcid.org/0000-0002-6566-0881>

References

- [1] Lüscher M 1991 *Nucl. Phys. B* **354** 531
- [2] Rummukainen K and Gottlieb S 1995 *Nucl. Phys. B* **450** 397
- [3] Christ N H, Kim C and Yamazaki T 2005 *Phys. Rev. D* **72** 114506
- [4] Bernard V, Lage M, Meißner U-G and Rusetsky A 2008 *J. High Energy Phys.* **JHEP08(2008)024**
- [5] He S, Feng X and Liu C 2005 *J. High Energy Phys.* **JHEP07(2005)011**
- [6] Lage M, Meißner U-G and Rusetsky A 2009 *Phys. Lett. B* **681** 439
- [7] Döring M, Meißner U-G, Oset E and Rusetsky A 2011 *Eur. Phys. J. A* **47** 139
- [8] Guo P, Dudek J, Edwards R and Szczepaniak A P 2013 *Phys. Rev. D* **88** 014501
- [9] Guo P 2013 *Phys. Rev. D* **88** 014507
- [10] Kreuzer S and Hammer H-W 2009 *Phys. Lett. B* **673** 260
- [11] Polejaeva K and Rusetsky A 2012 *Eur. Phys. J. A* **48** 67
- [12] Hansen M T and Sharpe S R 2014 *Phys. Rev. D* **90** 116003
- [13] Mai M and Döring M 2017 *Eur. Phys. J. A* **53** 240
- [14] Mai M and Döring M 2019 *Phys. Rev. Lett.* **122** 062503
- [15] Döring M, Hammer H-W, Mai M, Pang J-Y, Rusetsky A and Wu J 2018 *Phys. Rev. D* **97** 114508
- [16] Guo P 2017 *Phys. Rev. D* **95** 054508
- [17] Guo P and Gasparian V 2017 *Phys. Lett. B* **774** 441
- [18] Guo P and Gasparian V 2018 *Phys. Rev. D* **97** 014504
- [19] Guo P and Morris T 2019 *Phys. Rev. D* **99** 014501
- [20] Mai M, Döring M, Culver C and Alexandru A 2020 *Phys. Rev. D* **101** 054510
- [21] Guo P, Döring M and Szczepaniak A P 2018 *Phys. Rev. D* **98** 094502
- [22] Guo P 2020 *Phys. Lett. B* **804** 135370
- [23] Guo P and Döring M 2020 *Phys. Rev. D* **101** 034501
- [24] Guo P 2020 *Phys. Rev. D* **101** 054512
- [25] Guo P and Long B 2020 *Phys. Rev. D* **101** 094510
- [26] Guo P 2020 arXiv:2007.04473
- [27] Guo P and Long B 2020 *Phys. Rev. D* **102** 074508
- [28] Guo P 2020 *Phys. Rev. D* **102** 054514
- [29] Guo P and Gasparian V 2021 *Phys. Rev. D* **103** 094520
- [30] Guo P and Long B 2021 arXiv:2101.03901
- [31] Guo P 2021 *Phys. Rev. C* **103** 064611
- [32] Busch T, Englert B-G, Rzażewski K and Wilkens M 1998 *Found. Phys.* **28** 549–59
- [33] Stetcu I, Barrett B, van Kolck U and Vary J 2007 *Phys. Rev. A* **76** 063613
- [34] Stetcu I, Rotureau J, Barrett B R and van Kolck U 2010 *Ann. Phys., NY* **325** 1644
- [35] Rotureau J, Stetcu I, Barrett B, Birse M and van Kolck U 2010 *Phys. Rev. A* **82** 032711
- [36] Rotureau J, Stetcu I, Barrett B and van Kolck U 2012 *Phys. Rev. C* **85** 034003
- [37] Luu T, Savage M J, Schwenk A and Vary J P 2010 *Phys. Rev. C* **82** 034003
- [38] Yang C-J 2016 *Phys. Rev. C* **94** 064004
- [39] Johnson C W *et al* 2019 From bound states to the continuum: connecting bound state calculations with scattering and reaction theory (arXiv:1912.00451)
- [40] Zhang X 2020 *Phys. Rev. C* **101** 051602
- [41] Zhang X, Stroberg S R, Navrátil P, Gwak C, Melendez J A, Furnstahl R J and Holt J D 2020 *Phys. Rev. Lett.* **125** 112503
- [42] Miransky V A and Shovkovy I A 2015 *Phys. Rep.* **576** 1
- [43] Andersen J O, Naylor W R and Tranberg A 2016 *Rev. Mod. Phys.* **88** 025001
- [44] Fukushima K, Kharzeev D E and Warringa H J 2008 *Phys. Rev. D* **78** 074033
- [45] Adamczyk L *et al* (STAR) 2015 *Phys. Rev. Lett.* **114** 252302
- [46] Siddique I, Cao S, Tabassam U, Saeed M and Waqas M 2022 arXiv:2201.09634
- [47] Gusynin V P, Miransky V A and Shovkovy I A 1994 *Phys. Rev. Lett.* **73** 3499
Gusynin V P, Miransky V A and Shovkovy I A 1996 *Phys. Rev. Lett.* **76** 1005 (erratum)
- [48] Gusynin V P, Miransky V A and Shovkovy I A 1996 *Nucl. Phys. B* **462** 249
- [49] Chernodub M N 2010 *Phys. Rev. D* **82** 085011
- [50] Detmold W and Savage M J 2004 *Nucl. Phys. A* **743** 170
- [51] Detmold W 2005 *Phys. Rev. D* **71** 054506
- [52] Detmold W, Tiburzi B C and Walker-Loud A 2008 *PoS LATTICE2008* p 147
- [53] Detmold W, Tiburzi B C and Walker-Loud A 2009 *eCONF C0906083* p 03

- [54] Lee F X, Zhou L, Wilcox W and Christensen J C 2006 *Phys. Rev. D* **73** 034503
- [55] Lee F X, Kelly R, Zhou L and Wilcox W 2005 *Phys. Lett. B* **627** 71
- [56] Bali G S, Bruckmann F, Endrodi G, Fodor Z, Katz S D, Krieg S, Schafer A and Szabo K K 2012 *J. High Energy Phys.* **JHEP02(2012)044**
- [57] Bali G S, Bruckmann F, Endrodi G, Fodor Z, Katz S D and Schafer A 2012 *Phys. Rev. D* **86** 071502
- [58] Bruckmann F, Endrodi G and Kovacs T G 2013 *J. High Energy Phys.* **JHEP04(2013)112**
- [59] Bali G S, Bruckmann F, Endrodi G, Katz S D and Schäfer A 2014 *J. High Energy Phys.* **JHEP08(2014)177**
- [60] Bruckmann F, Endrodi G, Giordano M, Katz S D, Kovacs T G, Pittler F and Wellenhofer J 2017 *Phys. Rev. D* **96** 074506
- [61] Yamamoto A 2016 *Phys. Rev. Lett.* **117** 052001
- [62] Tiburzi B C 2013 *Phys. Rev. D* **88** 034027
- [63] Lujan M, Alexandru A, Freeman W and Lee F 2014 *Phys. Rev. D* **89** 074506
- [64] Freeman W, Alexandru A, Lujan M and Lee F X 2014 *Phys. Rev. D* **90** 054507
- [65] Niyazi H, Alexandru A, Lee F X and Lujan M 2021 *Phys. Rev. D* **104** 014510
- [66] Fukushima K, Ruggieri M and Gatto R 2010 *Phys. Rev. D* **81** 114031
- [67] Ferreira M, Costa P, Menezes D P, Providência C and Scoccola N N 2014 *Phys. Rev. D* **89** 016002
- [68] Tawfik A N and Magdy N 2014 *Phys. Rev. C* **90** 015204
- [69] Tawfik A N and Magdy N 2015 *Phys. Rev. C* **91** 015206
- [70] Tawfik A N 2016 *J. Phys.: Conf. Ser.* **668** 012082
- [71] Sanz-Cillero J J, Tawfik A N, Diab A M, Ezzelarab N and Shalaby A G 2016 *Adv. High Energy Phys.* **2016** 1381479
- [72] Tawfik A N, Diab A M and Hussein M T 2018 *J. Phys. G: Nucl. Part. Phys.* **45** 055008
- [73] Tawfik A N 2017 *Indian J. Phys.* **91** 93
- [74] Tawfik A N, Diab A M and Hussein M T 2019 *Chin. Phys. C* **43** 034103
- [75] Chaudhuri N, Ghosh S, Sarkar S and Roy P 2020 *Eur. Phys. J. A* **56** 213
- [76] Tawfik A N and Diab A M 2021 *Eur. Phys. J. A* **57** 200
- [77] Chaudhuri N, Ghosh S, Sarkar S and Roy P 2021 *Phys. Rev. D* **103** 096021
- [78] DLMF *NIST Digital Library of Mathematical Functions* ed D W Lozier, B I Schneider, R F Boisvert, C W Clark, B R Miller, B V Saunders, H S Cohl and M A McClain <http://dlmf.nist.gov/>, release 1.1.5 of 2022-03-15, F W J Olver, A B Olde Daalhuis, D W Lozier, B I Schneider, R F Boisvert, C W Clark, B R Miller, B V Saunders, H S Cohl, and M A McClain, eds.
- [79] Kasamanyan Z A, Gasparian V M and Yuzbashyan E S 1985 *Phys. Status Solidi b* **130** K149
- [80] Xiao D, Chang M-C and Niu Q 2010 *Rev. Mod. Phys.* **82** 1959
- [81] Kohmoto M 1985 *Ann. Phys., NY* **160** 343
- [82] Thouless D J, Kohmoto M, Nightingale M P and den Nijs M 1982 *Phys. Rev. Lett.* **49** 405
- [83] Hatsugai Y 1993 *Phys. Rev. Lett.* **71** 3697
- [84] Hatsugai Y 1993 *Phys. Rev. B* **48** 11851
- [85] Hatsugai Y 1997 *J. Phys.: Condens. Matter* **9** 2507
- [86] Shockley W 1939 *Phys. Rev.* **56** 317
- [87] Tamm I 1932 *Phys. Z. Sowjetunion* **1** 733
- [88] Harper P G 1955 *Proc. Phys. Soc. A* **68** 879
- [89] Berry M V 1984 *Proc. R. Soc. A* **392** 45
- [90] Simon B 1983 *Phys. Rev. Lett.* **51** 2167
- [91] Vanderbilt D 2018 *Berry Phases in Electronic Structure Theory: Electric Polarization, Orbital Magnetization and Topological Insulators* (Cambridge: Cambridge University Press)
- [92] Kohn W 1959 *Phys. Rev.* **115** 809
- [93] Heine V 1963 *Proc. Phys. Soc.* **81** 300